

On the observational characteristics of lithium-enhanced giant stars in comparison with normal red giants *

Yoichi TAKEDA¹ and Akito TAJITSU²

¹*National Astronomical Observatory, 2-21-1 Osawa, Mitaka, Tokyo 181-8588
takeda.yoichi@nao.ac.jp*

²*Subaru Telescope, 650 N. A'ohoku Place, Hilo, HI 96720, U.S.A.
tajitsu@subaru.naoj.org*

(Received 2017 April 12; accepted 2017 June 6)

Abstract

While lithium is generally deficient in the atmosphere of evolved giant stars because of the efficient mixing-induced dilution, a small fraction of red giants show unusually strong Li lines indicative of conspicuous abundance excess. With an aim to shed light on the origin of these peculiar stars, we carried out a spectroscopic study on the observational characteristics of selected 20 bright giants already known to be Li-rich from past studies, in comparison with the reference sample of a large number of normal late G –early K giants. Our special attention was paid to clarifying any difference between the two samples from a comprehensive point of view (i.e., with respect to stellar parameters, rotation, activity, kinematic properties, ${}^6\text{Li}/{}^7\text{Li}$ ratio, and the abundances of Li, Be, C, O, Na, S, and Zn). Our sample stars are roughly divided into “bump/clump group” and “luminous group” according to the positions on the HR diagram. Regarding the former group ($1.5 \lesssim \log(L/L_\odot) \lesssim 2$ and $M \sim 1.5\text{--}3 M_\odot$), Li-enriched giants and normal giants appear practically similar in almost all respect except for Li, suggesting that surface Li enhancement in this group may be a transient episode which normal giants undergo at certain evolutionary stages in their lifetime. Meanwhile, those Li-rich giants belonging to the latter group ($\log(L/L_\odot) \sim 3$ and $M \sim 3\text{--}5 M_\odot$) appear more anomalous in the sense that they tend to show higher rotation as well as higher activity, and that their elemental abundances (especially those derived from high-excitation lines) are apt to show apparent overabundances, though this might be due to a spurious effect reflecting the difficulty of abundance derivation in stars of higher rotation and activity. Our analysis confirmed considerable Be deficiency as well as absence of ${}^6\text{Li}$ as the general characteristics of Li-rich giants under study, which implies that engulfment of planets is rather unlikely for the origin of Li-enrichment.

Key words: stars: abundances — stars: activity — stars: atmospheres — stars: evolution — stars: late-type — stars: rotation

1. Introduction

While lithium (Li, $Z = 3$) is an important element in the spectroscopy of late-type stars (e.g., for investigating physical processes of stellar interiors), studying its abundance is not necessarily easy for red giant stars (low-to-intermediate mass stars of lower surface temperature and larger radius, which have evolved off the main sequence after exhaustion of core hydrogen). That is, this element generally suffers considerable deficiency in the atmosphere of these evolved stars, due to (1) destruction of Li atoms at the hot stellar interior of $T \gtrsim 2.5 \times 10^6$ K and (2) efficient evolution-induced mixing at the red-giant stage causing Li dilution in the outer envelope, by which the observable Li line is considerably weakened and its abundance determination becomes rather difficult (see e.g., Liu et al. 2014 and the references therein for representative Li abundance studies of red giants in general published so far).

Interestingly, however, a small proportion ($\sim 1\%$) of red

giants are known to show exceptionally strong Li lines, indicating a conspicuous overabundance of Li (by $\sim 1\text{--}2$ dex or even larger) compared to normal giants. Since these chemically peculiar stars, called “Li-rich giants,” attracted interest of astrophysicists, a number of studies have been published so far (see, e.g., Charbonnel & Balachandran 2000; Lèbre et al. 2009; Carlberg et al. 2010; Kumar et al. 2011; Monaco et al. 2011; Martell & Shetrone 2013; Silva Aguirre et al. 2014; Reddy & Lambert 2016; Casey et al. 2016; and the references therein). Nonetheless, the reason why such significant amount of Li atoms are existent in their atmospheres (unlike other normal giants) has not been clarified yet, though various mechanisms have been proposed so far (cf. the references mentioned above): e.g., internal production of fresh Li atoms by the reaction of ${}^3\text{He}(\alpha, \gamma){}^7\text{Be}(e^-, \nu){}^7\text{Li}$ (so-called Cameron–Fowler mechanism) followed by an efficient transport to the surface (for which several different processes are proposed), substantial supply of Li atoms by some external process such as swallowing of planets or brown dwarfs as a result of expansion in the red giant stage, or “insufficient dilution” by which much of the

* Based on data collected at Subaru Telescope, operated by the National Astronomical Observatory of Japan.

original Li is still retained at the surface of Li-rich giants which appear superficially peculiar compared to other normal giants, etc.

In any event, much more observational work would have to be done before we can reasonably understand the origin of this peculiarity, given that available information on their characteristics is still insufficient. Especially, comprehensive studies for a number of these peculiar giants in comparison with a large sample of normal giants seem to have been rarely done so far. That is, by observationally elucidating the similar and dissimilar aspects of these two groups from a diversified point of view, we may be able to find a clue for understanding the origin of Li peculiarity.

Conveniently, our group recently conducted extensive spectroscopic studies on a large number of normal red giants: Takeda, Sato, and Murata (2008; hereinafter referred to as Paper I) determined the stellar parameters and elemental abundances of 322 late G–early K giants. Takeda and Tajitsu (2014; hereinafter referred to as Paper II) investigated the Be abundances of 200 giants (sub-sample of 322 giants mentioned above) by analyzing the Be II 3131 line in the UV region. Takeda et al. (2015a; hereinafter referred to as Paper III) extensively studied the abundances of O (along with C and Na) for 239 giants (sub-sample of 322 giants mentioned above). Similarly, the abundances of S and Zn for these 239 giants were established by Takeda et al. (2016b; hereinafter referred to as Paper IV).

Given this situation, we decided to carry out a spectroscopic study on the observational characteristics of selected 20 Li-rich giants, based on high-dispersion spectra of wide wavelength coverage obtained by Subaru/HDS in almost the same manner as done for normal giants in Papers I–IV, by which we can compare the atmospheric parameters (T_{eff} , $\log g$, \dots), stellar parameters (e.g., L or $v_e \sin i$), kinematic parameters (such as space velocities relative to LSR, etc.), and abundances of Li, Be, C, O, Na, S, and Zn between these two groups.

The specific checkpoints we had in mind are as follows: — How are the stellar parameters of Li-rich giants compared with those of normal giants? Is there any difference in the position on the HR diagram between these groups? — What about the kinematic parameters characterizing the orbital motions in the Galaxy? Is there any difference in stellar populations?

— Do they have any special characteristics regarding active stellar properties such as rotational velocities or magnetic activity?

— We want to determine the Li abundances of Li-rich giants as precisely as possible. How are they compared with those of normal giants? Are the abundance distributions both groups connected continuously or clearly separated? — Can we detect any signature for the existence of ${}^6\text{Li}$ from the spectra of our program stars? Do these Li-rich giants show similar enrichment in Be? These two checkpoints would make an important touchstone to verify the planet accretion hypothesis.

— Do the abundances of light elements (C, O, Na), which may be affected by deep mixing, show any special trend?

— How about the abundance tendency of S and Zn? If Li enrichment is produced by accretion of rocky materials, some abundance peculiarity might be observed in these volatile species.

In addition, motivated by the necessity of establishing the key properties of the reference sample which were not addressed in our previous papers, we newly conducted a new supplementary analysis for the large sample of normal giants regarding Li abundance determination and stellar activity estimation, as separately described in appendix 1 (activity indices of 239 field giants) and appendix 2 (Li abundances of 239 field giants and 103 *Kepler* giants).

2. Observational data

The list of our program stars (20 Li-rich giants; most of them are apparently bright as $V \lesssim 8$ mag) is presented in table 1, which were selected from the compilation of Casey et al. (2016; cf. table 1 therein, which they published as online material). All these targets have already been investigated in previous studies (cf. table 1), of which we can make use for comparison or supplementary purposes. Above all, Kumar, Reddy, and Lambert’s (2011) paper is important, since 16 stars (out of 20) are included in their study, which may be referenced for the properties not touched in this paper (e.g., ${}^{12}\text{C}/{}^{13}\text{C}$ ratio).

The spectroscopic observations of these targets were carried out by using the High Dispersion Spectrograph (HDS; Noguchi et al. 2002) placed at the Nasmyth platform of the 8.2-m Subaru Telescope on 2016 October 12–13 (UT; two first half-nights).

On October 12, the standard Ub setting was adopted with the blue cross disperser, by which spectra of 13 stars (out of the 20 targets) covering 3000–4700 Å (resolving power was $R \simeq 60000$ with the use of 0."6 width slit) were obtained. The total exposure time per star was typically ~ 10 –20 min. In addition, HD 212430 was already observed with the same setting on 2013 July 17 (cf. Paper II). Accordingly, UV spectra are available for 14 stars (but not for HD 174104, HD 232862, KIC 9821622, HD 8676, PDS 100, and HD 6665).

On October 13, the standard Ra setting was adopted with red cross disperser, which resulted in spectra covering 5100–7800 Å (resolving power was $R \simeq 80000$ with the use of image slicer #2). The total exposure time per star was typically a few minutes to ~ 10 min.

The reduction of the spectra (bias subtraction, flat-fielding, scattered-light subtraction, spectrum extraction, wavelength calibration, co-adding of frames to improve S/N, continuum normalization) was performed by using the “echelle” package of the software IRAF¹ in a standard manner.

Regarding the finally obtained UV spectra (October 12 observation), the typical S/N ratio at the Be II 3131 line region is around ~ 50 ($\lesssim 100$). As to the yellow–red re-

¹ IRAF is distributed by the National Optical Astronomy Observatories, which is operated by the Association of Universities for Research in Astronomy, Inc. under cooperative agreement with the National Science Foundation.

gion spectra (October 13 observation), sufficiently high S/N ratios could be accomplished; i.e., regarding the Li I 6708 region, S/N \sim 500–1000 for most stars, except for HD 232862 (\sim 200), KIC 9821622 (\sim 90), and PDS 100 (\sim 250).

3. Atmospheric parameters

Our determination of atmospheric parameters [effective temperature (T_{eff}), surface gravity ($\log g$), microturbulence (v_t), and metallicity ($[\text{Fe}/\text{H}]$)] was implemented in the same manner as in Paper I (see subsection 3.1 therein for the details) based on the equivalent widths (W_λ) of Fe I and Fe II lines measured on the spectrum of each star.

Unlike the case of normal field giants studied in Paper I, the spectral lines of several stars (especially HD 174104, HD 21018, HD 232862, and HD 170527) turned out to be appreciably rotationally-broadened. In such cases, a special fitting function (constructed by appropriately merging the rotational- and Gaussian-broadening functions) was used for W_λ measurement (if the lines are not so broadened, the conventional Gaussian-fitting method was adopted). Even so, regarding such Li-rich giants of broad lines, measuring W_λ was considerably difficult due to the blending effect and the number of available lines was small (which eventually lead to less reliable solutions).

The resulting atmospheric parameters are summarized in table 1, while the $A(\text{Fe})$ values (Fe abundances corresponding to the final solutions) are plotted against W_λ and χ_{low} in figure 1, where we can see that there is no systematic dependence. The detailed W_λ and $A(\text{Fe})$ data for each star are given in tableE1.dat (supplementary online material). The internal statistical errors involved with these solutions are \sim 20–70 K, \sim 0.1–0.3 dex, \sim 0.1–0.4 km s $^{-1}$, and \sim 0.05–0.1 dex for T_{eff} , $\log g$, v_t , and $[\text{Fe}/\text{H}]$, respectively, which tend to be somewhat larger than the case of Paper I. The model atmosphere for each star to be used in this study was generated by interpolating Kurucz’s (1993) ATLAS9 model grid in terms of T_{eff} , $\log g$, and $[\text{Fe}/\text{H}]$.

The mutual correlations of these atmospheric parameters are depicted in figure 2, where Li-rich giants (this study) and normal giants (Paper I) are shown in large open circles and small filled circles, respectively. We summarize some notable characteristics read from this figure: — Generally speaking, many of our program stars occupy parameter ranges almost consistent with those of the normal giants studied in Paper I, with a few exceptions as explained below.

— Three stars (HD 30834, HD 205349, and HD 787) have T_{eff} as low as \sim 4000–4300 K, while no normal giants in Paper I have T_{eff} lower than \sim 4500 K.² In such cases, a meaningful comparison between both samples is difficult.

— A similar argument holds also for HD 205349 regarding

the surface gravity ($\log g = 0.89$), which is outside of the range ($1.5 \lesssim \log g \lesssim 3.5$) covered by the reference sample of Paper I.

— Our program stars of Li-rich giants have metallicities not much different from the solar value ($-0.3 \lesssim [\text{Fe}/\text{H}] \lesssim +0.3$), while the sample giants in Paper I include stars down to $[\text{Fe}/\text{H}] \sim -0.8$.

— One star (HD 232862) is a notable outlier, because its $\log g$ (3.79) is unusually large for a giant. Given that this star is one of the four broad-line stars mentioned above, it may be possible that our parameter solutions for this star are not reliable. Lèbre et al. (2009) adopted $T_{\text{eff}} = 5000(\pm 250)$ K, $\log g = 3.0(\pm 0.5)$, and $[\text{Fe}/\text{H}] = -0.30(\pm 0.1)$; and only $\log g$ is discrepant from ours. We note in table 1 that $B - V$ and T_{eff} of this star do not conform to the mean relation (i.e., too blue for its T_{eff}) According to SIMBAD, this star is remarked as “binary or multiple system” and thus Hipparcos parallax is not available, which may have something to do with this anomaly. In any event, the results for this star should be viewed with caution.

The T_{eff} , $\log g$, $[\text{Fe}/\text{H}]$, and v_t values (along with the luminosities and Li abundances to be addressed later in section 4 and section 7, respectively) we derived for 20 program stars are compared with available published values taken from various literature in figure 3. Generally speaking, a reasonable consistency is observed for most cases, though several considerably discrepant cases (such as $\log g$ for HD 232862 just mentioned) are also seen.

4. Evolutionary status

We derived the luminosity (L) from the apparent magnitude, distance, interstellar extinction, and bolometric correction (as done in Paper I; cf. subsection 3.2 therein) for 17 stars, for which Hipparcos parallaxes are available, where we used the newly reduced data (van Leeuwen 2007). The errors of parallaxes are on the order of \sim 10% for most stars, which correspond to \sim 0.1 dex in $\log L$. Only for HD 174104, however, a considerably large error is exceptionally expected, since its parallax data given in the catalogue is 0.75 ± 0.73 milliarcsec. The adopted parallax and the resulting L for each star are given in table 1. As seen from figure 3e, our $\log L$ values tend to be slightly higher (though not significant) than those derived by Charbonnel and Balachandran (2000) and Kumar et al. (2011), which may be due to their neglect of interstellar extinction effect.

Regarding 3 stars (HD 232862, KIC 9821622, PDS 100) where Hipparcos data are lacking, we tried to estimate the possible range of their L values by using the relation $L \propto T_{\text{eff}}^4 M/g$ along with the spectroscopically determined T_{eff} and $\log g$ plotted in figure 4a, from which we can guess M (stellar mass) by comparing them with the theoretical relations. Since we do not have much confidence with our parameter solutions of HD 232862 (cf. section 3), we tentatively take two largely different $\log g$ values (3.8 and 3.0) as upper and lower limits. Then, putting $M/M_\odot \sim 1$ and ~ 2 inferred from figure 4a for each limit.

² This is simply a matter of sample selection. The 322 red giants studied in Paper I were actually the targets of Okayama planet search program, where stars with $B - V < 1$ were preferentially selected (because the atmosphere of K giants with $B - V > 1$ turned out to be less stable from the preliminary study of radial-velocity monitoring).

we have $0.4 \lesssim \log(L/L_\odot) \lesssim 1.5$. As to KIC 9821622 and PDS 100, we estimate from figure 4a $M/M_\odot \simeq 2(\pm 0.5)$ and $M/M_\odot \simeq 3(\pm 1)$, which yield $1.42 < \log(L/L_\odot) < 1.64$ and $2.34 < \log(L/L_\odot) < 2.64$, respectively. We note that such evaluated L range for KIC 9821622 is consistent with the value (1.59 ± 0.10) derived by Jofré et al. (2015), while that for PDS 100 is appreciably higher than Reddy et al.’s (2002) estimation (1.65) quoted by Kumar et al. (2011).

The resulting $\log L$ vs. $\log T_{\text{eff}}$ diagram of 20 Li-rich giants stars are shown in figure 4b. We can see from this figure that our program stars are roughly divided into two groups:

— (i) Less luminous giants of $1.5 \lesssim \log(L/L_\odot) \lesssim 2$ with $T_{\text{eff}} \sim 4500\text{--}5000$ K, presumably belonging to either RGB bump stars or red-clump stars though these two classes are close to each other on the HR diagram and difficult to discriminate (see, e.g., fig. 2 of Kumar et al. 2011). A reasonable mass-range estimate of this group³ would be $M \sim 1.5\text{--}3 M_\odot$.

— (ii) Luminous giants of $\log(L/L_\odot) \sim 3$, which probably have masses around $M \sim 3\text{--}5 M_\odot$ according to the comparison with theoretical evolutionary tracks. We note that their T_{eff} values tend to separately cluster around ~ 5500 K and ~ 4000 K in our sample.

For convenience, we will hereinafter call these groups “bump/clump group” and “luminous group” respectively. Actually, this division is not only an apparent position-based classification but also has an intrinsic significance (cf. section 6 or section 9).

5. Kinematic properties

As done in Paper I, we computed the kinematic parameters of 17 program stars (for which Hipparcos data are available) following the procedure described in Takeda (2007; cf. subsection 2.2 therein). The resulting parameters (which are given in tableE2.dat of the online material) are compared with those of the normal giants in figure 5, where the correlations of z_{max} (maximum separation from the galactic plane) vs. V_{LSR} (rotation velocity component relative to the Local Standard of Rest: LSR), e (orbital eccentricity) vs. $\langle R_g \rangle$ (mean galactocentric radius), and $|\mathbf{v}_{\text{LSR}}|$ ($\equiv \sqrt{U_{\text{LSR}}^2 + V_{\text{LSR}}^2 + W_{\text{LSR}}^2}$; amplitude of the velocity vector relative to LSR) vs. $[\text{Fe}/\text{H}]$, are shown. The following statements can be made by inspecting figure 5:

— Most of our Li-rich giants belong to the thin-disk population (one possible exception may be HD 12203, which might be of the thick-disk origin due to its rather large z_{max} (0.82 kpc), just like those found by Monaco et al. (2011).

— We can recognize that the distributions of these

parameters for the Li-rich sample and the normal sample are essentially the same, which suggests that kinematic factors are essentially irrelevant to the origin of Li-rich phenomenon.

— We observe in figure 5c that the $|\mathbf{v}_{\text{LSR}}|$ values of our program stars reasonably show a decreasing tendency with $[\text{Fe}/\text{H}]$ (as in normal giants) even in such a rather narrow metallicity range ($-0.3 \lesssim [\text{Fe}/\text{H}] \lesssim +0.3$).

6. Rotation and activity

The projected rotational velocities ($v_e \sin i$) of 20 Li-rich giants were evaluated in the same manner as in Paper I (cf. subsection 4.2 therein) from the macrobroadening width determined by the 6080–6089 Å fitting (cf. table 2 for more information), while subtracting the contributions of instrumental broadening as well as $\log g$ -dependent macroturbulence broadening [cf. eq. (1) in Paper I]. Regarding four stars (HD 174104, HD 21018, HD 232862, and HD 170527) where rotation is apparently dominant, we applied the rotational broadening function instead of the Gaussian approximation adopted in Paper I. Such established spectrum fitting for each star is demonstrated in figure 6a.

We also determined the activity-sensitive index $\log R'_{\text{Kp}}$ for 14 program stars with available UV spectra (cf. section 2), where R'_{Kp} is the ratio of the chromospheric emission flux of Ca II K line at 3933.66 Å (after being subtracted by the photospheric flux computed from the relevant model atmosphere) to the total bolometric flux, following the procedure detailed in Takeda et al. (2012; cf. section 3 therein). The spectra in the core region of Ca II K line, on which this measurement was made, are depicted in figure 6b.⁴ Similarly, we also evaluated $\log R'_{\text{Kp}}$ for 200 normal giants, for which UV spectra are available (cf. Paper II), in order to compare the activity nature of these two samples with each other. This supplementary analysis is described in appendix 1.

The resulting $v_e \sin i$ as well as $\log R'_{\text{Kp}}$ are plotted against T_{eff} in figure 6c,d (for both Li-rich and normal samples), and their mutual correlation is shown in figure 6e. We can see the following trends from these figures:

— A positive correlation between $\log R'_{\text{Kp}}$ and $v_e \sin i$ is observed (figure 6e), which is reasonable since the magnetic activity of dynamo origin is rotation-dependent.

— We see a tendency that rotation and activity tend to become lower with a decrease in T_{eff} (figure 6c,d), which is already known and presumably due to an enhanced magnetic braking effect (see, e.g., fig. 18.24 of Gray 2005).

³ As recently concluded by Takeda and Tajitsu (2015), the mass results derived in Paper I are likely to be appreciably overestimated for many stars, especially for those in the red-clump region where tracks of different masses are complicatedly intersected. This is the reason why we did not derive M for each star, unlike Paper I. Therefore, what we can state is only a rough estimate regarding the possible range of M .

⁴ The parameter (α) controlling the integration range [$w_{\text{min}}(\equiv 3933.7 - \alpha)$, $w_{\text{max}}(\equiv 3933.7 + \alpha)$] for evaluating the core-emission strength was chosen to be $\alpha = 0.9$ Å as the standard value, while wider values of $\alpha = 2.4, 1.4,$ and 1.9 Å were adopted for HD 21018, HD 9746, and HD 205349, respectively. Regarding HD 170527 which shows an exceptionally strong activity among the present sample, the integration was performed in an especially wide range of [3929 Å, 3938 Å].

— It is evident that a large fraction of Li-rich giants have considerably larger $v_e \sin i$ compared to normal giants (figure 6c,d).

— However, this is not necessarily a general trend. Actually, not a few Li-rich giants surely follow almost the same $v_e \sin i$ distribution (i.e., low scale of $\lesssim 5 \text{ km s}^{-1}$) as the case of normal giants. Interestingly, most of these ordinary (slower) rotators belong to the “bump/clump” group, while the unusual (rapider) rotators tend to be in the “luminous” group (though some exceptions do exist; e.g., HD 170527 has large $v_e \sin i$ as well as low $\log L$). We will return to this point again in section 9.

7. Analysis of Li 6708 and 6104 lines

The Li abundances of 20 program stars were determined from two line features of neutral lithium, the resonance line at $\sim 6707.8 \text{ \AA}$ ($2s^2S-2p^2P^o$) and the subordinate line at 6103.6 \AA ($2p^2P^o-3d^2D$). We employed almost the same procedure for abundance determination as adopted in our previous papers (e.g., Paper III or Paper IV), which consists of three consecutive steps: (i) LTE synthetic spectrum fitting based on the numerical technique described in Takeda (1995) to derive the abundance of target element as well as those of other relevant elements (cf. table 2), (ii) inverse evaluation of the equivalent width (W) for the line feature of interest (cf. table 3), and (iii) determination of LTE (A^L) as well as non-LTE (A^N) abundances from such obtained W , from which non-LTE correction $\Delta^N (\equiv A^N - A^L)$ can also be derived. We used Kurucz’s (1993) WIDTH9 program for calculations of A and W , which was considerably modified to enable analysis of multi-component lines as well as to include the non-LTE effect.

Regarding the 6704–6711 \AA fitting including Li I 6708, we used the line data given in table 2 of Smith, Lambert, and Nissen (1998) in the 6707.2–6708.1 \AA region as done by Takeda and Kawanomoto (2005), supplemented by the data taken from the VALD database (Ryabchikova et al. 2015) outside of this range (though only the Fe I 6708.2819 line was neglected because VALD’s $\log gf$ value for this line turned out unreasonably too large). Meanwhile, we adopted the data compiled in VALD for the 6101–6105 \AA fitting (including Li I 6104). In both cases, we primarily considered only lines of ^7Li while neglecting ^6Li in our analysis, because no signature was recognized for the existence of ^6Li as mentioned below in this section. The finally accomplished spectrum fitting in these two wavelength regions is shown in figure 7.

The non-LTE departure coefficients necessary for deriving non-LTE abundances were computed on the parameter grid of T_{eff} from 4000 K to 5500 K, $\log g$ from 0.0 to 4.0, $A(\text{Li})$ from 0.0 to 4.0, and $[\text{Fe}/\text{H}] = 0$ by following the same procedure described in Takeda and Kawanomoto (2005), and applied to each star by interpolation. The trends of the non-LTE corrections are illustrated in figure 8, where the results for 239 normal giants (separately described in appendix 2) are also shown for the case of Li I 6708. We can see from figure 8a,b that our Δ^N val-

ues are consistent with those published by Lind, Asplund, and Barklem (2009). We also note that the behavior of Δ_{6708}^N for Li-rich giants are different from those of Δ_{6104}^N (for both Li-rich and Li-poor case) and Δ_{6708}^N (for normal Li-poor case), in the sense that the former is strongly $A(\text{Li})$ -dependent and turns from positive to negative with an increase in $A(\text{Li})$ (figure 8e), while the latter is generally positive and weakly T_{eff} -dependent (figure 8c,d). The reason for this tendency is explained in figure 9a, where we can see that the non-LTE effect for the Li 6708 line acts in the direction of line-weakening (mainly due to the overionization effect lowering the line opacity: $l_0^{\text{NLTE}}/l_0^{\text{LTE}} < 1$) and $\Delta_{6708}^N > 0$ for the normal Li-poor case (solid line), while the dilution of the line source function ($S_l/B < 1$) begins as the abundance increases (dashed line) which leads to a line-strengthening and negative Δ_{6708}^N . In contrast, such a dilution of S_l never occurs for the weak Li I 6104 line (cf. figure 9b), for which Δ_{6104}^N is always positive.

We first investigated whether our Li-rich giants have any ^6Li in their atmospheres, which is important as a touchstone of “external” hypothesis. That is, this lighter isotope (which is more easily processed than ^7Li and not expected to exist in normal giants) would be detected if swallowing of planets (presumably consisting of materials with $^6\text{Li}/^7\text{Li} \sim 0.1$ as observed in the interstellar matter or in meteorites) is the cause for Li enrichment. Although this is usually a quite delicate and difficult task if based on line profiles alone.⁵ We can make use of the fact that Li abundances derived from the strongly saturated Li I 6708 line are sensitive to this isotope ratio while that from the weak Li 6104 line is essentially inert. The variations of Li abundances (δA) for each line caused by increasing $^6\text{Li}/^7\text{Li}$ from 0.0 to 0.1 are plotted against W and T_{eff} in figure 10a and figure 10b, respectively. It is apparent from figure 10a that the extent of δA_{6708} is appreciably large and W -dependent, while δA_{6104} is negligibly small ($\simeq 0.0$). This sensitivity difference causes a manifest distinction in the A_{6104}^N vs. A_{6708}^N diagram shown in figure 10c ($^6\text{Li}/^7\text{Li} = 0.0$) and figure 10d ($^6\text{Li}/^7\text{Li} = 0.1$), from which we can see that inclusion of ^6Li brings about an apparent inconsistency between the abundances derived from two lines.⁶ Accordingly, we conclude that there is no sign of ^6Li in our program stars. In the remainder of this paper, our discussion on the Li abundances is exclusively confined to those obtained with $^6\text{Li}/^7\text{Li} = 0.0$.

The results of the Li abundances (A_{6708} and A_{6104}) are summarized in table 4, while more detailed data (including W and Δ^N) are given in tableE3.dat of the online material. Our A_{6708}^L values are mostly in reasonable agree-

⁵ Reddy et al. (2002) and Reddy and Lambert (2016) carried out such a detailed profile analysis of Li I 6708 line for Li-rich giants (PDS 100 and HD 16771) and found that ^6Li is almost absent, which is consistent with our consequence.

⁶ This conclusion is qualitatively the same as derived by Balachandran et al. (2000) for HD 9746 (one of our program stars with the strongest W_{6708} of 468 m \AA). However, their $|\delta A|$ values appear to be quantitatively larger than ours (for both Li I 6708 and 6104 lines; cf. table 5 therein), to which the difference in the atomic line data or in the atmospheric parameters may be attributed.

ment with the published results (cf. figure 3f). The trends of W and $A(\text{Li})$ for both lines in terms of T_{eff} , $[\text{Fe}/\text{H}]$ and $v_e \sin i$ are plotted in figure 11. The following characteristics are read from this figure.

— The W_{6708} values of Li-rich giants are markedly strong ($\sim 100\text{--}500 \text{ m}\text{\AA}$) compared to those of normal giants (several tens of $\text{m}\text{\AA}$ or less) (figure 11a).

— The Li abundances of 20 Li-rich giants range from ~ 1.9 to ~ 3.8 , some of which (e.g., HD 8676, HD 10437, HD 9746) exceed the solar-system value (3.31).

— A weak trend of decreasing $A(\text{Li})$ with a decrease in T_{eff} is observed (figure 11b), which may be due to the selection effect in defining Li-rich giants (i.e., for the same W , $A(\text{Li})$ becomes smaller as T_{eff} is lowered).

— Regarding the Li abundances of 20 program stars, no appreciable dependence is observed upon $[\text{Fe}/\text{H}]$ (figure 11c) as well as $v_e \sin i$ (figure 11d), though normal giants tend to show a weak dependence of $A(\text{Li})$ upon $[\text{Fe}/\text{H}]$ as well as $v_e \sin i$.

— Interestingly, the distribution of A_{6708}^{N} for normal giants ($-1 \lesssim A(\text{Li}) \lesssim 2$) continuously connect with that of Li-rich giants ($\sim 1.9\text{--}3.8$).

The errors in A_{6708}^{N} (for Li-rich giants) due to uncertainties of atmospheric parameters were estimated to be $\sim 0.1\text{--}0.2$ dex (for a T_{eff} change of 100 K), $\lesssim 0.02$ dex (for a $\log g$ change of 0.3 dex), and from ~ 0.01 dex [$W_{6708} \sim 100 \text{ m}\text{\AA}$] to ~ 0.1 dex [$W_{6708} \sim 400\text{--}500 \text{ m}\text{\AA}$] (for a v_t change of 0.4 km s^{-1}), which means that T_{eff} plays the most important role in the accuracy of Li abundances.

8. Beryllium abundance

We tried to determine the Be abundances of 14 Li-rich giant stars (for which UV spectra are available) by analyzing the $3130.65\text{--}3131.35 \text{ \AA}$ region comprising the Be II 3131.066 line (line of ^9Be , because we did not consider unstable ^7Be in the analysis) in same manner as done in Paper II for 200 normal giants. However, the Be abundance solution for the spectrum fitting (shown in figure 12a) was obtained for only 5 stars (HD 203136, HD 212430, HD 12203, HD 194937, and HD 167304), while it failed to converge for the remaining 9 stars (i.e., all what we can say about their Be abundances do not exceed the upper limit of $\lesssim -1$; cf. Paper II). Moreover, the W_{3131} values of two stars (HD 12203, HD 167304) out of these successful 5 stars are only $\sim 2\text{--}3 \text{ m}\text{\AA}$ and almost on the same order of the upper limit values; thus their abundances are near to the detection limit and unreliable (i.e., class-c in Paper II). Regarding the representative case of HD 194937, another theoretical spectrum corresponding to the solar-system Be abundance (1.42) is also overplotted in figure 12a (dashed line) in order to demonstrate the difference.

The resulting W_{3131} vs. T_{eff} , $A(\text{Be})$ vs. T_{eff} , and $A(\text{Be})$ vs. $[\text{Fe}/\text{H}]$ relations for these 5 stars (as well as the those of normal giants derived in Paper II) are plotted in figure 12d, figure 12e, and figure 12f, respectively. We can see from these figures the following characteristics regard-

ing the Be abundances of Li-rich giants:

— As in the case of normal giants (Paper II), photospheric Be abundances of Li-rich giants are considerably deficient (by $\sim 1\text{--}2$ dex or more) compared to the solar-system abundance (1.42).

— That is, there is no difference in the behavior of Be abundances between the Li-rich giant sample and normal giant sample, which means that whichever mechanism causing Li-enrichment in red giants does not affect Be.

— In particular, the possibility of Be overabundance is ruled out. This is consistent with the consequences already reported by previous investigations (e.g., de Medeiros et al. 1997, Castilho et al. 1999, Melo et al. 2005), though these past studies failed to determine the Be abundances in practice (i.e., what they could derive was only the upper limits).

— This can be confirmed from figure 12b,c, where the spectra of two Li-rich giant are compared with those of normal Li-poor giants with similar atmospheric parameters. We can not discern any meaningful difference in the spectrum feature at the position of Be II lines.

— This argument holds not only for ^9Be II lines but also for the lines of ^7Be II (unstable isotope with a half-decay time of 53 days), for which we can not recognize any signature in the spectra. (Note that the apparent features at the wavelengths of two ^7Be II 3130.58 and 3131.23 lines are mostly due to OH and Fe I, which are equally seen for Li-rich as well as normal giants.) It is thus unlikely that Li is being produced near to the photosphere of Li-rich giants by the ^7Li synthesis process via ^7Be (e.g., by explosive phenomenon such as classical novae, as recently reported by Tajitsu et al. 2015).

9. Abundances of C, O, Na, S, and Zn

We determined the abundances of C, O, and Na for the program stars from C I 5380, [O I] 6300⁷ as well as O I 7771–5, and Na I 6160 lines by following the same procedure as described in Paper III. Similarly, the S and Zn abundances were derived from S I 6757 and Zn I 6362 lines in the same manner as done in Paper IV. The information regarding the spectrum fitting and equivalent-width evaluation for each case is summarized in table 2 and table 3. How the fitted theoretical spectrum matches the observed spectrum is displayed for each star in figure 13. The finally obtained abundances relative to the Sun $[X/\text{H}]$ ($X = \text{C}, \text{O}, \text{Na}, \text{S}, \text{or Zn}$) are given in table 4, while more detailed data (including W and Δ^{N}) are presented in tableE3.dat of the online material. The results of W , Δ^{N} , and $[X/\text{H}]$ for each line are plotted against T_{eff} in figure 14, where the $[X/\text{Fe}]$ vs. $[\text{Fe}/\text{H}]$ relation is also shown (for both Li-rich giant and normal giant samples).

A significant tendency regarding the abundances of Li-rich giants can be noticed by inspection of figure 14, especially in the $[X/\text{Fe}]$ vs. $[\text{Fe}/\text{H}]$ plots. That is, we see a number of considerably discrepant points (toward di-

⁷ Regarding the blending effect of the Ni I 6300.35 line on this [O I] line, we took its contribution into account by assuming $[\text{Ni}/\text{H}] = [\text{Fe}/\text{H}]$.

rection of overabundance in most cases) in their $[X/Fe]$ ratios (open circles) derived from C I 5380, O I 7774, Na I 6161, and Zn I 6362 in comparison to those of normal giants (filled circles), while such a trend is not observed for [O I] 6300 and S I 6757. Yet, we note that $[X/Fe]$ ratios (for any element) for an appreciable fraction of Li-rich sample stars still show a good agreement with those of normal sample at the same $[Fe/H]$. In order to investigate the origin of this problem more in detail, we plot the difference $\delta[X/Fe]$ (deviation from the mean trend depicted as straight lines in figure 14) against the star number for each star in figure 15, where the corresponding T_{eff} , $\log L$, $v_e \sin i$, and $\log R'_{\text{Kp}}$ are also shown. Interestingly, the following characteristics can be seen from figure 15:

— The Li-rich giants showing conspicuously large $\delta[X/Fe]$ generally have large $v_e \sin i$, which are divided into higher T_{eff} group ($\gtrsim 4800$ K, ~ 20 – 30 km s $^{-1}$, such as star #1, #2, #4, and #7) and lower T_{eff} group ($\lesssim 4500$ K, ~ 5 – 10 km s $^{-1}$, such as stars #14–#20).

— In contrast, those Li-rich stars for which $\delta[X/Fe]$ is fairly small and insignificant for any element and indiscernible from normal giants are slow rotators ($v_e \sin i$ only up to a few km s $^{-1}$; e.g., star #5, #6, #8–#13).

— When we examine the $\log L$ and T_{eff} of these two groups (figure 15b) along with the classification mentioned in section 4, we see that the former (rapid rotator) group and the latter (slow rotator) group tend to be associated with the “luminous Li-rich giants” and “bump/clump Li-rich giants”, respectively. This means that those two groups, which were discriminated by the positions on the HR diagram, have different characteristics also from the viewpoint of abundance determination.

Accordingly, regarding the question “Do Li-rich giants show any significant difference in the abundance trend of C, O, Na, S, or Zn compared to normal giants?”, we may state that those Li-rich giants of the latter slowly-rotating group are quite similar to the normal sample with respect to the abundance behavior of these elements.

Yet, the situation is more complicated for the former group of higher rotational velocities, which show apparently discrepant $[X/Fe]$ for several specific elements compared to normal giants. This may imply the existence of abundance peculiarities (mostly overabundances) also in elements other than Li in this group of Li-rich giants. However, we can not exclude a possibility that this is nothing but a superficial effect; i.e., these abundances are not correct. Let us focus on oxygen, for example, where $[O/Fe]_{6300}$ is almost normal but $[O/Fe]_{7774}$ is anomalously large in these stars. This reminds us of the well-known trend that high-excitation O I 7771–5 lines are especially strengthened in stars with high chromospheric activity (i.e., higher temperature in the upper layer) and the O abundance derived from these triplet lines by using normal radiative-equilibrium model atmospheres is appreciably overestimated (such as seen in Hyades K-type stars, e.g., section 3 in Takeda 2008 and the references therein). Actually, recent investigation by Dupree, Avrett, and Kurucz (2016) has shown that such a strengthening of activity-origin occurs in the O I triplet lines also for gi-

ants. If this interpretation is correct, rotation-induced activity might have yielded apparent overestimation of $[O/Fe]_{7774}$ in this group of large $v_e \sin i$. It is not clear, however, whether all the other $[X/Fe]$ showing considerably large discrepancy (e.g., $[C/Fe]_{5380}$, $[Na/Fe]_{6161}$, $[Zn/Fe]_{6362}$) are explained by this scenario. As another possibility, inevitably increased abundance errors for the case of broad/shallow/blended line spectra might also (at least partly) be involved. In any case, we are not sure at present whether they represent the true abundances; they might simply reflect the difficulty of abundance determination for such Li-rich giants of high rotation and high activity.

10. Summary and discussion

We carried out a comprehensive study on various observed properties (stellar parameters, rotation, activity, kinematic parameters, chemical abundances of Li, Be, C, O, Na, S, and Zn) of 20 Li-enhanced giants and compared them with those of a large sample of normal red giants. The purpose was to clarify what is different or not different between these two samples. The resulting observational characteristics are summarized below.

- We found from the stellar parameters that our program stars are roughly divided into (i) “bump/clump group” ($1.5 \lesssim \log(L/L_{\odot}) \lesssim 2$, $M \sim 1.5$ – $3 M_{\odot}$) and (ii) “luminous group” ($\log(L/L_{\odot}) \sim 3$; $M \sim 3$ – $5 M_{\odot}$) from their positions on the HR diagram.
- From the viewpoint of kinematic parameters, most of our Li-rich sample stars belong to the thin-disk population, such as in the reference sample of normal red giants. This is consistent with the spectroscopically established metallicities, which are not much different from the solar metallicity ($-0.3 \lesssim [Fe/H] \lesssim +0.3$).
- With regard to $v_e \sin i$ and $\log R'_{\text{Kp}}$, our program stars of the “luminous group” show a tendency of rotating more rapidly (and more active) as compared to the sample of normal giants, while those of the “bump/clump group” are quite indistinctive in this respect (mostly slow rotators).
- Regarding the lithium abundances derived from Li I 6708 and Li I 6104 lines, we found that inclusion of ${}^6\text{Li}$ (${}^6\text{Li}/{}^7\text{Li} = 0.1$) causes a systematic disagreement between these two, while consistency can be accomplished for the case of ${}^6\text{Li}/{}^7\text{Li} = 0.0$. This suggests that ${}^6\text{Li}$ is absent in the atmospheres of Li-rich giants in general.
- As to the abundance of beryllium, the resulting $A(\text{Be})$ values are $A(\text{Be}) \lesssim 0$ at most, indicating an appreciable deficiency as was the case for normal giants (Paper II). In this sense, we do not see any distinct difference of $A(\text{Be})$ between the Li-rich and the normal samples; especially, the possibility of Be overabundance is ruled out.
- Regarding the abundances of C, O, Na, S, and Zn in comparison with the sample of normal giants,

the abundance trend of slow rotators (mostly in the “bump/clump group”) is practically similar and almost indiscernible. Meanwhile, considerably discrepant abundances are seen for some elements (e.g., those from high-excitation lines) in Li-rich giants of faster rotators (mostly in the “luminous group”), though they might be superficial results caused by a non-classical chromospheric effect or by increased difficulties of abundance determination,

In concluding this paper, we make some comments on the possible Li-enrichment mechanism, which is still under debate, based on the observational evidences elucidated from this study.

Firstly, we could not recognize any signature of ${}^6\text{Li}$, and confirmed that Be is deficient as in normal giants, which means that any peculiarities in ${}^6\text{Li}$ as well as in Be are not accompanied with the overabundance of Li. Accordingly, “planet-engulfment hypothesis” (accretion of unprocessed gas or solid material) is considered to be unlikely as the origin of Li-rich giants (at least as a major mechanism), since it would enrich Be as well as ${}^6\text{Li}$.

Secondly, the fact that our program stars are roughly divided into two groups “luminous group” (rapid rotator of higher activity, higher-mass stars of $\sim 3\text{--}5 M_{\odot}$) and “bump/clump group” (slow rotator of lower activity, less massive stars of $M \sim 1.5\text{--}2.5 M_{\odot}$) may suggest that different origins are responsible for their Li anomaly.

Regarding the former group, many of them have larger $v_e \sin i$ and thus are more active as compared to the normal giants of similar T_{eff} . It seems likely that high rotation is the important key to understand their Li-rich phenomenon. Actually, the connection between rotation and high Li content was already remarked by some previous studies (e.g., Fekel & Balachandran 1993, Drake et al. 2002, de Laverny et al. 2003). Can rapid rotation itself lead to an overabundance of Li in the surface (e.g., enhanced mixing)? Or large angular momentum is simply a by-product of some other Li-enrichment process?

As to the latter “bum/clump” group, their stellar properties appear almost similar to those of normal giants. That being a case, the surface Li enhancement in this group might be a very short-lived episode which normal giants undergo in a certain period in their lifetime, as has been occasionally suggested (e.g., Charbonnel & Balachandran 2000). Then, the question is, at which evolutionary stage does this phenomenon takes place: At the bump in the first ascent of RGB, or at the He core flash at the tip of RGB (cf. Kumar et al. 2011)? Maybe both are probable, since we know two Li-rich giants in the *Kepler* field with seismologically established evolutionary status: KIC 9821622 (locating near to the RGB bump) is in the H-shell burning stage (Jofré et al. 2015), while KIC 5503307 is a clump star in the He-burning stage (Silva Aguirre et al. 2014).

This research has been carried out by using the SIMBAD database, operated by CDS, Strasbourg, France.

Appendix 1. Ca II 3934 core-emission strengths of 200 red giants

In order to compare the behavior of $\log R'_{\text{KP}}$ for the 14 Li-rich giants derived in section 6 with that of normal giants, we determined this parameter for 200 giants (sub-sample of 322 stars in Paper I), for which UV spectra used for Be abundance determinations in Paper II are available. Since these data contain the violet region including Ca II 3933.66 line, we derived $\log R'_{\text{KP}}$ by integrating the core emission component of this line in the same manner as done in section 6 by following the procedure detailed in Takeda et al. (2012). The spectra of 200 stars in the relevant region are displayed in figure 16. The resulting $\log R'_{\text{KP}}$ values are compiled in tableE4.dat of the online material, where more detailed data (atmospheric parameters and projected rotational velocity taken from Paper I, integration range) are also given. These $\log R'_{\text{KP}}$ data are shown in figure 6d,e (filled circles).

Appendix 2. Li abundances of normal red giants

In an attempt to compare the Li abundances of 20 Li-rich giants (cf. section 7) with those of normal giants, we determined $A(\text{Li})$ from Li I 6708 line also for the following two samples: (1) 239 giants studied in Paper III and Paper IV (subsample of 322 stars in Paper I), for which red-region spectra are available. (2) 103 giants in the *Kepler* field investigated in the stellar parameter studies by Takeda and Tajitsu (2015) and Takeda et al. (2016a), for which the evolutionary status is asteroseismologically established. The adopted procedure is essentially the same as adopted in section 7, though the spectrum fitting was done in a slightly narrower region of 6707.0–6708.5 Å (because especially broad-line stars are not included in this case). We could achieve satisfactory convergence for most cases, though the solutions failed for the cases where the Li line feature is too weak and undetectable (8 out of 239 giants, 17 out of 103 *Kepler* giants). The accomplished fit between theoretical and observed spectra are shown in figure 17 (239 field giants) and figure 18 (103 *Kepler* giants). The resulting Li abundances and the related quantities (W_{6708} , Δ_{6708}^{N} , etc) and presented in tableE5.dat and tableE6.dat of the online material, respectively, and their trends are shown in figure 19. The Δ_{6708}^{N} , W_{6708} , and $A_{6708}^{\text{N}}(\text{Li})$ values for the former 239 giants are also plotted (in light-blue dots) in figure 8 and figure 11 as the reference data of normal giants.

Since all the 239 stars in the former sample are included in Liu et al.’s (2014) extensive Li abundance analysis for red giants, we can compare our results (LTE Li abundances and non-LTE corrections) with theirs as displayed in figure 19a,b. We can see from figure 19a that our Li abundances are quite consistent with those of Liu et al. (2014) as far as the Li I 6708 line is sufficiently strong (group A1). However, as the line becomes weaker (group A2), their abundances tend to be systematically larger than our results. The non-LTE corrections adopted by Liu

et al. (2014), for which they invoked Lind et al.'s (2009) tables, are slightly (by a few hundredths dex) smaller than ours (figure 19b), though the differences are quantitatively insignificant.

Let us briefly discuss the trends of Li abundances in these (239+103) giant stars. Here, it should be remarked that all the converged abundance solutions are not necessarily reliable, because they may include fortuitously converged cases even if the Li line is negligibly weak. Following Takeda and Kawanomoto (2005), we estimate the detectability limit of W_{6708} as being on the order of several mÅ which corresponds to $A(\text{Li}) \sim 0$ (cf. figure 19c). Therefore, the abundance values of $A(\text{Li}) \lesssim 0$ are below the reliability limit (shown by a dotted line in figure 19c,d,e,f), and thus should not be seriously taken. We can see that Li abundance distributions of both samples (239 field giants and 103 *Kepler* giants) are almost similar to each other (cf. figure 19d,e,f). That is, $A(\text{Li})$ shows a large dispersion ($\gtrsim 2$ dex) and a weak decreasing tendency with a decrease in T_{eff} (figure 19d) as well as in $v_e \sin i$ (figure 19f). This may be related to the correlation between $v_e \sin i$ and T_{eff} (figure 19g), though the declining trend of $A(\text{Li})$ with a lowering of T_{eff} in *Kepler* RG stars (cf. figure 19d, red filled circles) may reflect the evolution of Li dilution during the course of ascending RGB. No appreciable dependence upon $[\text{Fe}/\text{H}]$ is recognized (figure 19e).

Regarding the *Kepler* giants (with known mass values and evolutionary status), $v_e \sin i$ tends to increase with M (figure 19h) and the dispersion of $A(\text{Li})$ (and $v_e \sin i$) is notably small at $M \sim 1.8 M_{\odot}$ around the RC1–RC2 boundary (figure 19i), which is interesting. KIC 5503307, one of our *Kepler* sample showing a prominently strong Li I 6708 line (figure 18), is a Li-rich giant discovered by Silva Aguirre et al. (2014), which is classified as RC1 (red-clump star of M lower than $1.8 M_{\odot}$ burning He in its core). Considering that KIC 9821622 (also studied in our main analysis) is a Li-rich giant known to be in the RG stage (i.e., H shell-burning star ascending RGB; cf. Jofré et al. 2015), we can understand that Li-rich phenomenon in red giants takes place in both red-giant branch stars and red-clump stars.

References

- Balachandran, S. C., Fekel, F. C., Henry, G. W., & Uitenbroek, H. 2000, *ApJ*, 542, 978
- Barrado y Navascués, D., De Castro, E., Fernández-Figueroa, M. J., Cornide, M., & Garcia-López, R. J. 1998, *A&A*, 337, 739
- Bressan, A., Marigo, P., Girardi, L., Salasnich, B., Dal Cero, C., Rubele, S., & Nanni, A. 2012, *MNRAS*, 427, 127
- Bressan, A., Marigo, P., Girardi, L., Nanni, A., & Rubele, S. 2013, *EPJ Web of Conferences*, 43, 3001 (DOI: <http://dx.doi.org/10.1051/epjconf/20134303001>)
- Brown, J. A., Sneden, C., Lambert, D. L., & Dutchover, E., Jr 1989, *ApJS*, 71, 293
- Carlberg, J. K., Smith, V. V., Cunha, K., Majewski, S. R., & Rood, R. T. 2010, *ApJ*, 723, L103
- Casey, A. R., et al. 2016, *MNRAS*, 461, 3336
- Castilho, B. V., Spite, F., Barbuy, B., Spite, M., de Medeiros, J. R., & Gregorio-Hetem, J. 1999, *A&A*, 345, 249
- Charbonnel, C., & Balachandran, S. C. 2000, *A&A*, 359, 563
- de Laverny, P., do Nascimento, J. D., Jr., Lèbre, A., & De Medeiros, J. R. 2003, *A&A*, 410, 937
- de Medeiros, J. R., Lebre, A., de Garcia Maia, M. R., & Monier, R. 1997, *A&A*, 321, L37
- Drake, N. A., de la Reza, R., da Silva, L., & Lambert, D. L. 2002, *AJ*, 123, 2703
- Dupree, A. K., Avrett, E. H., & Kurucz, R. L. 2016, *ApJ*, 821, L7
- ESA, 1997, *The Hipparcos and Tycho Catalogues*, ESA SP-1200,
- Fekel, F. C., & Balachandran, S. 1993, *ApJ*, 403, 708
- Gray D. F. 2005, *The Observation and Analysis of Stellar Photospheres*, 3rd ed. (Cambridge, Cambridge University Press)
- Jofré, E., Petrucci, R., García, L., & Gómez, M., 2015 *A&A*, 584, L3
- Kumar, Y. B., Reddy, B. E., & Lambert, D. L. 2011, *ApJ*, 730, L12
- Kurucz, R. L. 1993, *Kurucz CD-ROM No.13* (Cambridge: Smithsonian Astrophysical Observatory) [available at (<http://kurucz.harvard.edu/cdroms.html>)]
- Kurucz, R. L., & Bell B. 1995, *Kurucz CD-ROM, No. 23* (Cambridge: Smithsonian Astrophysical Observatory) [available at (<http://kurucz.harvard.edu/cdroms.html>)]
- Lèbre, A., Palacios, A., do Nascimento, J. D., Jr, Konstantinova-Antova, R., Kolev, D., Aurière, M., de Laverny, P., & De Medeiros, J. R. 2009, *A&A*, 504, 1011
- Lind, K., Asplund, M., & Barklem, P. S. 2009, *A&A*, 503, 541
- Liu, Y. J., Tan, K. F., Wang, L., Zhao, G., Sato, B., Takeda, Y., & Li, H. N. 2014, *ApJ*, 785, 94
- Luck, R. E. 1982, *PASP*, 94, 811
- Martell, S. L., & Shetrone, M. D. 2013, *MNRAS*, 430, 611
- Melo, C. H. F., de Laverny, P., Santos, N. C., Israelian, G., Randich, S., Do Nascimento, J. D., Jr, de Medeiros, J. R. 2005, *A&A*, 439, 227
- Monaco, L., et al. 2011, *A&A*, 529, A90
- Noguchi, K. et al. 2002, *PASJ*, 54, 855
- Primas, F., Duncan, D. K., Pinsonneault, M. H., Deliyannis, C. P., Thorburn, J. A. 1997, *ApJ*, 480, 784
- Reddy, A. B. S., & Lambert, D. L., 2016, *A&A*, 589, A57
- Reddy, B. E., Lambert, D. L., Hrivnak, B. J., & Bakker, E. J., 2002, *AJ*, 123, 1993
- Ryabchikova, T., Piskunov, N., Kurucz, R. L., Stempels, H. C., Heiter, U., Pakhomov, Yu., & Barklem, P. S. 2015, *Phys. Scr.*, 90, 054005
- Silva Aguirre, V., et al. 2014, *ApJ*, 784, L16
- Smith, V. V., Lambert, D. L., & Nissen, P. E. 1998, *ApJ*, 506, 405
- Tajitsu, A., Sadakane, K., Naito, H., Arai, A., & Aoki, W., 2015, *Nature*, 518, 381
- Takeda, Y. 1995, *PASJ*, 47, 287
- Takeda, Y. 2007, *PASJ*, 59, 335
- Takeda, Y. 2008, in *The Metal-Rich Universe*, eds. G. Israelian & G. Meynet, (Cambridge: Cambridge University Press), 308
- Takeda, Y., & Honda, S. 2005, *PASJ*, 57, 65
- Takeda, Y., & Kawanomoto, S. 2005, *PASJ*, 57, 45
- Takeda, Y., Kawanomoto, S., & Sadakane, K. 1998, *PASJ*, 50, 97
- Takeda, Y., Omiya, M., Harakawa, H., & Sato, B. 2016b, *PASJ*, 68, 81 (Paper IV)

- Takeda, Y., Sato, B., & Murata, D. 2008, PASJ, 60, 781
(Paper I)
- Takeda, Y., Sato, B., Omiya, M., & Harakawa, H. 2015a,
PASJ, 67, 24 (Paper III)
- Takeda, Y., & Tajitsu, A. 2014, PASJ, 66, 91 (Paper II)
- Takeda, Y., & Tajitsu, A. 2015, MNRAS, 450, 397
- Takeda, Y., Tajitsu, A., Honda, S., Kawanomoto, S., Ando,
H., & Sakurai, T. 2012, PASJ, 64, 130
- Takeda, Y., Tajitsu, A., Sato, B., Liu, Y.-J., Chen, Y.-Q., &
Zhao, G. 2016a, MNRAS, 457, 4454
- van Leeuwen, F. 2007, Hipparcos, the New Reduction of the
Raw Data (Berlin: Springer)

Table 1. Basic data and the stellar parameters of 20 Li-rich giants.

#	name	HIP	Sp	V	$B-V$	π	$\log L$	T_{eff}	$\log g$	v_t	[Fe/H]	$v_e \sin i$	$\log R'_{\text{KP}}$	Reference
(1)	(2)	(3)	(4)	(5)	(6)	(7)	(8)	(9)	(10)	(11)	(12)	(13)	(14)	(15)
1	HD 174104	92223	G0 Ib	8.36	0.72	0.75	3.26	5649	2.05	2.33	-0.14	28.7	...	L82
2	HD 21018	15807	G5 III	6.37	0.85	2.68	2.72	5327	2.05	1.81	+0.07	21.2	-4.70	BN98, CB00, KRL11
3	HD 203136	105208	K0	7.74	0.94	3.77	1.98	5084	2.80	1.17	+0.14	5.1	-4.74	CB00, KRL11
4	HD 232862	...	G8 II	9.60	0.73	4938	3.79	2.02	-0.20	20.2	...	L09
5	HD 212430	110602	K0 III	5.76	0.97	7.11	2.07	4923	2.48	1.32	-0.19	2.0	-5.00	L14
6	KIC 9821622	4896	2.91	1.03	-0.25	1.9	...	J15
7	HD 170527	90274	K0	6.84	1.00	6.31	1.71	4842	2.57	1.63	-0.35	22.9	-3.69	KRL11
8	HD 12203	9343	G5	6.75	1.00	6.57	1.74	4812	2.49	1.33	-0.32	2.0	-4.95	KRL11
9	HD 194937	100953	G9 III	6.23	1.07	10.59	1.52	4786	2.56	1.23	-0.03	1.8	-5.11	KRL11
10	HD 8676	6647	K0 III	7.77	1.05	4.27	1.71	4774	2.53	1.26	-0.11	1.8	...	KRL11
11	HD 183492	95822	K0 III	5.57	1.05	10.90	1.78	4765	2.58	1.25	+0.06	2.0	-5.21	B89, CB00, KRL11
12	HD 167304	89246	K0 III	6.36	1.04	6.07	1.97	4761	2.43	1.35	+0.04	2.8	-5.21	KRL11
13	HD 10437	8052	K1 III	6.57	1.08	6.74	1.92	4756	2.55	1.28	0.00	1.9	-5.09	KRL11
14	HD 214995	112067	K0 III:	5.92	1.11	11.78	1.58	4626	2.43	1.25	+0.04	4.9	-4.96	KRL11
15	PDS 100	4524	1.98	1.46	-0.05	8.3	...	KRL11
16	HD 6665	5285	G5	8.44	1.19	4.49	1.57	4520	2.61	1.23	+0.28	5.2	...	CB00, KRL11
17	HD 9746	7493	K1 III:	6.20	1.24	6.36	2.11	4490	2.14	1.40	-0.10	7.2	-4.55	B89, B00, CB00, KRL11
18	HD 30834	22678	K3 III	4.79	1.41	5.41	2.92	4283	1.79	1.45	-0.24	2.3	-5.04	B89, CB00, KRL11
19	HD 205349	106420	K1 Ibvar	6.27	1.80	2.45	3.27	4138	0.89	2.24	-0.18	6.5	-5.38	B89, CB00, KRL11
20	HD 787	983	K4 III	5.29	1.48	5.25	2.75	4027	1.75	1.31	+0.07	2.8	-5.56	B89, CB00, KRL11

(1) Object number (arbitrarily assigned). (2) Star name. (3) Hipparcos number. (4) Spectral type. (5) V magnitude. (6) $B-V$ color. (7) Hipparcos parallax (in milliarcsec) (van Leeuwen 2007). (8) Logarithmic luminosity (in unit of L_{\odot}). (9) Effective temperature (in K). (10) Logarithmic surface gravity (in cm s^{-2}). (11) Microturbulent velocity dispersion (in km s^{-1}). (12) Fe abundance relative to the Sun (in dex). (13) Projected rotational velocity (in km s^{-1}). (14) Logarithmic ratio of the chromospheric Ca II 3934 line core emission flux to the total bolometric flux (cf. Takeda et al. 2012). (15) Previous papers where the object was studied (or referred to). The targets are arranged in the order of decreasing T_{eff} . The spectral type and the photometric data (V and $B-V$) were adopted from the Hipparcos catalogue (ESA 1997), except for those of HD 232862 which were taken from the SIMBAD database. Note that UV spectra (and thus $\log R'_{\text{KP}}$) are not available for six stars (#1, #4, #6, #10, #15, #16) and parallax data are lacking for three stars (#4, #6, #15). The reference codes given in column (15) (they are by no means complete, because some of them are based on other studies; each paper should be consulted for more details) denote as follows: L82 — Luck (1982), B89 — Brown et al. (1989), BN98 — Barrado y Navacué et al. (1998), CB00 — Charbonnel and Balachandran (2000), B00 — Balachandran et al. (2000), L09 — Lèbre et al. (2009), KRL11 — Kumar et al. (2011), L14 — Liu et al. (2014), J15 — Jofré et al. (2015).

Table 2. Spectrum fitting analysis done in this study.

Purpose	fitting range (Å)	abundances varied*	atomic data source	figure
$v_e \sin i$ determination	6080–6089	Si, Ti, V, Fe, Co, Ni	KB95 (cf. Paper I)	figure 6a
Li abundance from Li I 6708	6704–6711	Li, Fe	SLN98+VALD (cf. section 7)	figure 7a
Li abundance from Li I 6104	6101–6105	Li, Ca, Fe	VALD (cf. section 7)	figure 7b
Be abundance from Be II 3131	3130.65–3131.35	Be, Ti, Fe	P97 (cf. Paper II)	figure 12a
C abundance from C I 5380	5378.5–5382	C, Ti, Fe, Co	KB95 (cf. Paper III)	figure 13a
O abundance from [O I] 6300	6297–6303	O, Si, Sc, Fe	TH05+KB95 (cf. Paper III)	figure 13b
O abundance from O I 7771–5	7770–7777	O, Fe, Nd, CN	TKS98+KB95 (cf. Paper III)	figure 13c
Na abundance from Na I 6161	6157–6164	Na, Ca, Fe, Ni	KB95 (cf. Paper III)	figure 13d
S abundance from S I 6757	6756.0–6758.1	S, Fe, Co	KB95 (cf. Paper IV)	figure 13e
Zn abundance from Zn I 6362	6361–6365	O, Cr, Fe, Ni, Zn	KB95 (cf. Paper IV)	figure 13f

* The abundances of other elements than these were fixed by assuming $[X/H] = [\text{Fe}/H]$ in the fitting. KB95 — Kurucz and Bell (1995), SLN98 — Smith, Lambert, and Nissen (1998), VALD — VALD database (Ryabchikova et al. 2015), P97 — Primas et al. (1997), TH05 — Takeda and Honda (2005), and TKS98 — Takeda, Kawanomoto, and Sadakane (1998).

Table 3. Line data adopted for evaluating the equivalent widths.

line	W	λ (Å)	χ_{low} (eV)	$\log gf$ (dex)	Remark
Li I 6708	W_{6708}	6707.756	0.00	-0.427	${}^7\text{Li}$
		6707.768	0.00	-0.206	${}^7\text{Li}$
		6707.907	0.00	-0.932	${}^7\text{Li}$
		6707.908	0.00	-1.161	${}^7\text{Li}$
		6707.919	0.00	-0.712	${}^7\text{Li}$
		6707.920	0.00	-0.932	${}^7\text{Li}$
		(6707.920)	(0.00)	(-0.479)	${}^6\text{Li}$
		(6707.923)	(0.00)	(-0.178)	${}^6\text{Li}$
Li I 6104	W_{6104}	6103.540	1.848	+0.072(+0.03)	${}^7\text{Li}$
		6103.651	1.848	+0.327(+0.03)	${}^7\text{Li}$
		6103.665	1.848	-0.627(+0.03)	${}^7\text{Li}$
		(6103.574)	(same as 6103.540)		${}^6\text{Li}$
		(6103.686)	(same as 6103.651)		${}^6\text{Li}$
		(6103.699)	(same as 6103.665)		${}^6\text{Li}$
Be II 3131	W_{3131}	3131.066	0.000	-0.468	${}^9\text{Be}$
C I 5380	W_{5380}	5380.337	7.685	-1.842	
[O I] 6300	W_{6300}	6300.304	0.000	-9.717	
O I 7774	W_{7774}	7774.166	9.146	+0.174	
Na I 6161	W_{6161}	6160.747	2.104	-1.260	
S I 6757	W_{6757}	6756.851	7.870	-1.760	
		6757.007	7.870	-0.900	
		6757.171	7.870	-0.310	
Zn I	W_{6362}	6362.338	5.796	+0.150	

See table 2 for the reference sources of these line data. Regarding the line data for ${}^6\text{Li}$ (which was eventually neglected in our main analysis), we consulted SLN98 and VALD for the 6708 and 6104 lines, respectively. Since the gf values for the ${}^7\text{Li}$ 6104 lines given in VALD are scaled according to the isotope ratio of ${}^7\text{Li}/{}^6\text{Li} \simeq 12$ (typical value for Interstellar matter), we recovered the true gf values by adding a slight correction of +0.03 dex.

Table 4. Resulting abundances of Li, Be, C, O, Na, S, and Zn.

# (1)	name (2)	[Fe/H] (3)	$A_{\text{Li}67}$ (4)	$A_{\text{Li}61}$ (5)	$A_{\text{Be}31}$ (6)	[C] ₅₃₈₀ (7)	[O] ₆₃₀₀ (8)	[O] ₇₇₇₄ (9)	[Na] ₆₁₆₁ (10)	[S] ₆₇₅₇ (11)	[Zn] ₆₃₆₂ (12)
1	HD 174104	-0.14	3.17	3.35	...	-0.23	...	+0.31	-0.23	-0.24	+0.13
2	HD 21018	+0.07	2.93	3.29	...	-0.37	-0.72	+0.21	+0.23	-0.11	+0.38
3	HD 203136	+0.14	2.40	2.40	0.07	-0.23	-0.24	+0.11	+0.36	-0.07	+0.06
4	HD 232862	-0.20	2.57	2.86	...	+0.43	...	+0.41	-0.12	...	+0.19
5	HD 212430	-0.19	1.94	1.80	-0.63	-0.38	-0.27	-0.16	+0.12	-0.19	-0.18
6	KIC 9821622	-0.25	1.85	1.67	...	-0.25	+0.07	-0.01	-0.18	-0.11	-0.14
7	HD 170527	-0.35	3.24	3.31	...	-0.27	-0.42	+0.76	-0.31	-0.68	-0.06
8	HD 12203	-0.32	2.14	2.12	-1.74	-0.16	+0.02	+0.08	-0.15	-0.13	-0.14
9	HD 194937	-0.03	3.15	3.01	-0.44	-0.21	-0.05	-0.19	+0.08	-0.01	-0.19
10	HD 8676	-0.11	3.81	3.56	...	-0.23	-0.12	-0.05	-0.03	-0.14	-0.08
11	HD 183492	+0.06	2.28	2.20	...	-0.13	+0.04	+0.09	+0.14	+0.05	+0.26
12	HD 167304	+0.04	2.79	2.79	-1.42	-0.19	+0.00	+0.10	+0.36	+0.16	+0.12
13	HD 10437	0.00	3.62	3.44	...	-0.32	+0.08	+0.02	+0.11	+0.07	+0.07
14	HD 214995	+0.04	3.06	3.13	...	+0.21	-0.14	+0.23	+0.09	+0.14	+0.39
15	PDS 100	-0.05	2.59	2.62	...	+0.15	-0.25	+0.80	+0.46	-0.14	+0.19
16	HD 6665	+0.28	2.80	2.92	...	+0.56	+0.24	+0.52	+0.47	+0.38	+0.74
17	HD 9746	-0.10	3.73	3.90	...	+0.18	-0.15	+0.48	+0.03	-0.04	+0.00
18	HD 30834	-0.24	2.63	2.53	...	+0.14	+0.02	-0.08	+0.18	-0.14	-0.31
19	HD 205349	-0.18	1.88	2.00	...	+0.02	-0.13	+0.22	+0.85	-0.42	+0.36
20	HD 787	+0.07	2.03	2.53	...	+1.19	+0.22	+0.22	+0.57	...	+0.26

Following the star number, star name, and metallicity (Fe/H) in Columns (1)–(3) (the same data as in table 1), the NLTE Li abundances derived from Li I 6708 as well as Li I 6104 lines (on the condition of ${}^6\text{Li}/{}^7\text{Li} = 0.0$) are given in Columns (4) and (5), and the LTE Be abundance is in Column (6). (Note that these logarithmic number abundances relative to hydrogen are normalized in the usual manner as $A_{\text{H}} = 12.00$.) Columns (7)–(12) present the [X/H] values (differential abundances relative to the Sun in dex, defined as $A_{\text{star}}^{\text{X}} - A_{\text{O}}^{\text{X}}$) for C (from C I 5380, NLTE), O (from [O I] 6300, LTE), O (from O I 7774, NLTE), Na (from Na I 6161, NLTE), S (from S I 6757, NLTE), and Zn (from Zn I 6362), respectively.

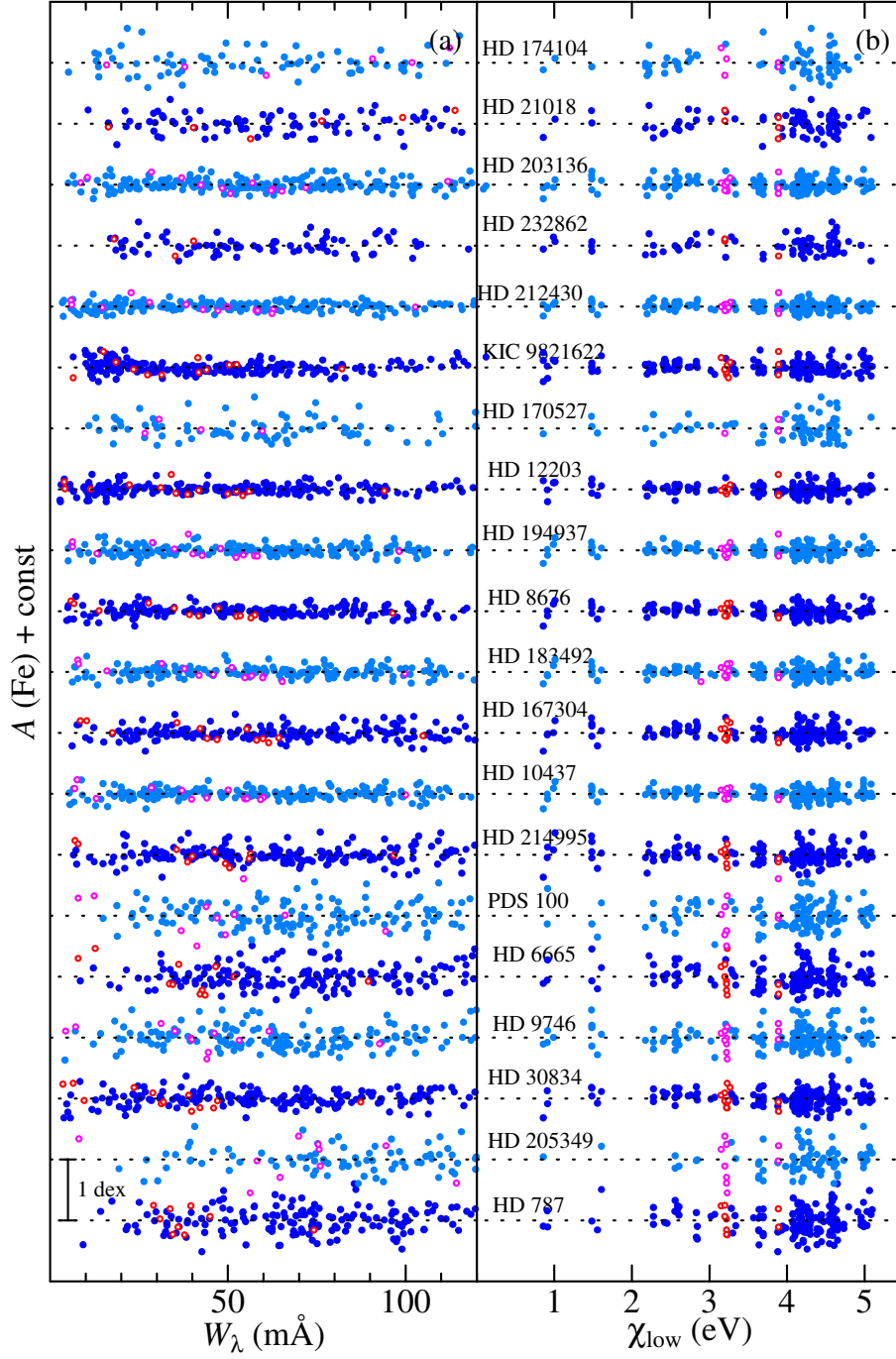


Fig. 1. Fe abundance vs. equivalent width relation (left panel (a)) as well as Fe abundance vs. lower excitation potential relation (right panel (b)) corresponding to the finally established atmospheric parameters of T_{eff} , $\log g$, and v_t for each of the 20 stars, being arranged in the decreasing order of T_{eff} as in table 1. The filled and open symbols correspond to Fe I and Fe II lines, respectively. The results for each star are shown relative to the mean abundance (indicated by the horizontal dotted line), and vertically shifted by 1.0 relative to the adjacent ones.

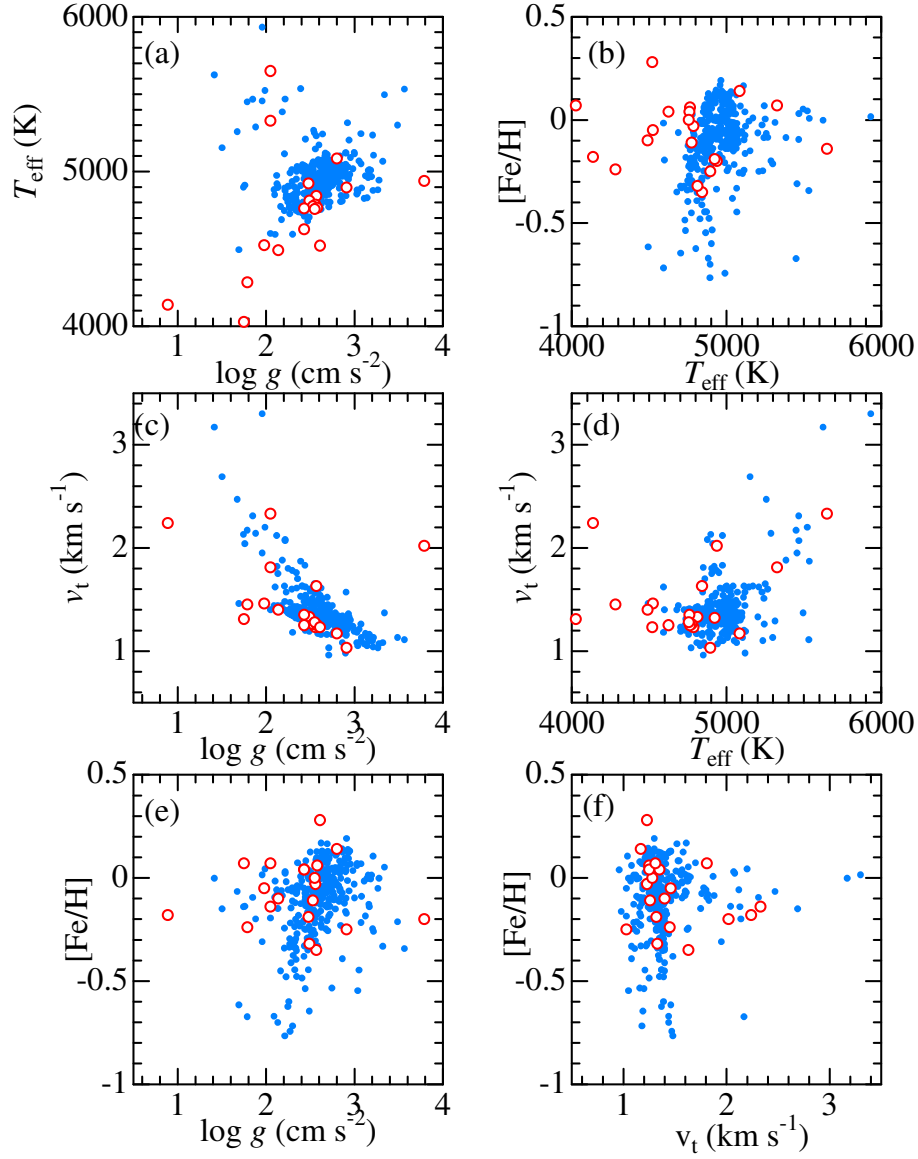


Fig. 2. Mutual correlations of the atmospheric parameters spectroscopically determined by using Fe I and Fe II lines for 20 Li-rich giants (this study; open circles) as well as 322 red giants (Paper I; filled circles). (a) T_{eff} vs. $\log g$, (b) $[\text{Fe}/\text{H}]$ vs. T_{eff} , (c) v_t vs. $\log g$, (d) v_t vs. T_{eff} , (e) $[\text{Fe}/\text{H}]$ vs. $\log g$, and (f) $[\text{Fe}/\text{H}]$ vs. v_t .

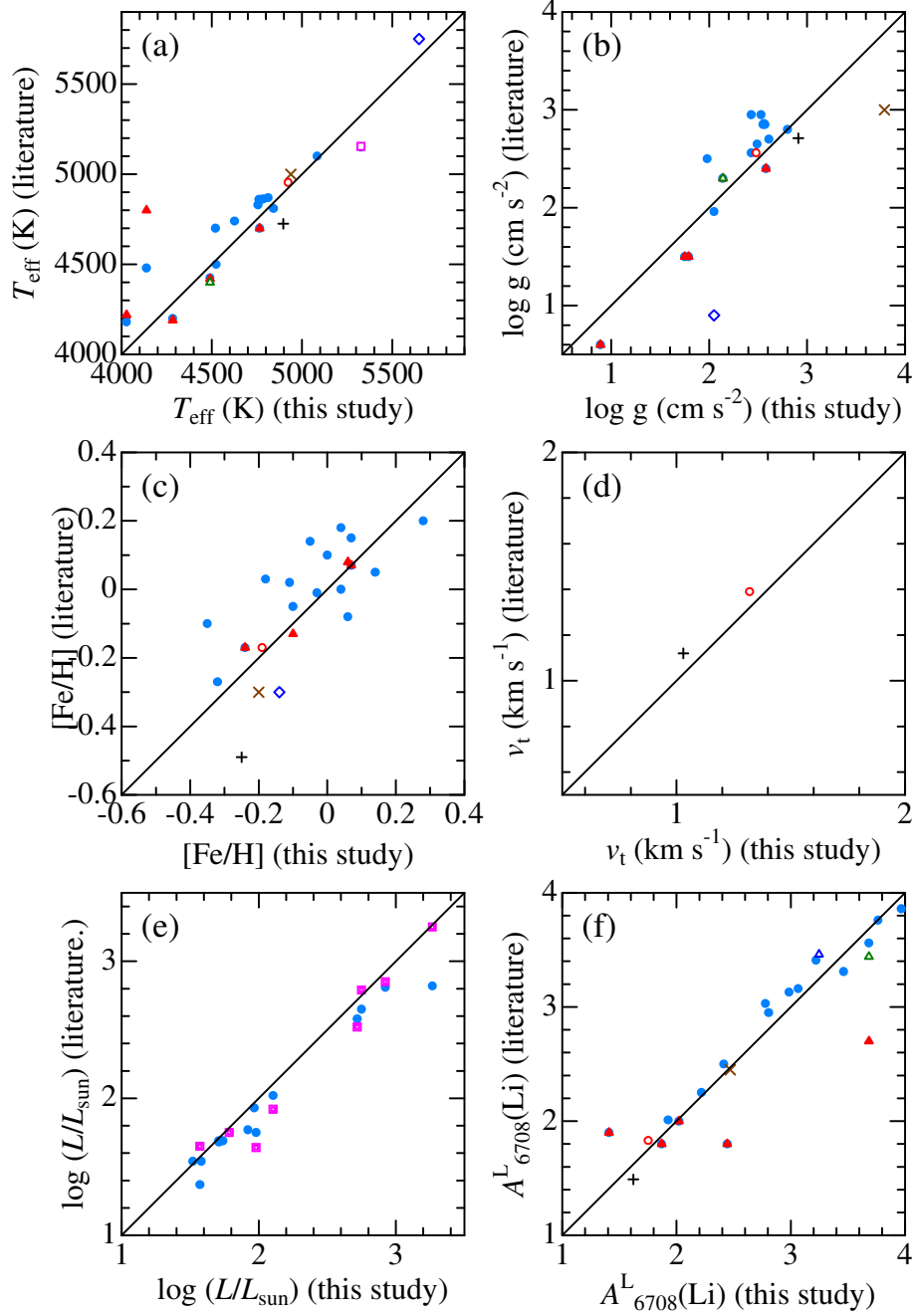


Fig. 3. Comparison of the stellar parameters (and Li abundance) determined in this study with those reported by previous studies: (a) T_{eff} , (b) $\log g$, (c) $[\text{Fe}/\text{H}]$, (d) v_t , (e) $\log(L/L_{\odot})$, and (f) $A_{6708}^{\text{L}}(\text{Li})$ (LTE abundance derived from Li I 6708). Most of the published data were taken from table 1 of Casey et al. (2016), though some data were newly added by ourselves (e.g., v_t , $\log L$). Each symbol corresponds to different literature source (see the caption of table 1 for the meanings of the abbreviations): Filled circles (blue) — KRL11, filled triangles (red) — B89, open circle (red) — L14, open triangle (green) — B00, open square (pink) — BN98, open diamond (blue) — L82, double square (pink) — CB00, Greek cross (black, +) — J15, and St. Andrew's cross (brown, ×) — L09. Regarding the microturbulence of HD 174104, our v_t (2.3 km s^{-1}) is largely different from L82's value (5 km s^{-1}), and thus is not included in panel (d).

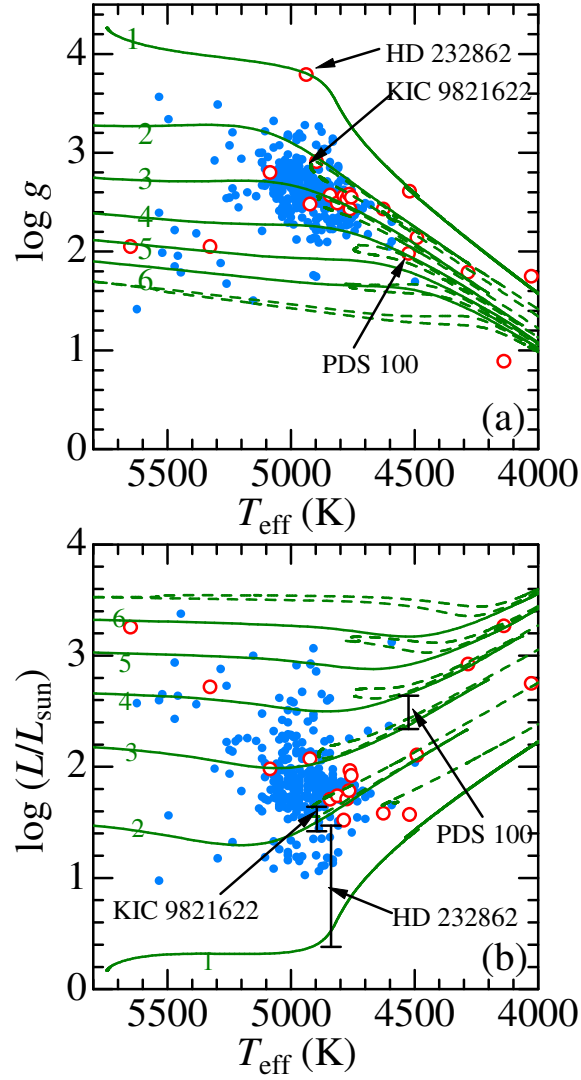


Fig. 4. The $\log g$ vs. T_{eff} (upper panel (a)) and $\log(L/L_{\odot})$ vs. T_{eff} (lower panel (b)) diagrams based on the parameters of 20 Li-rich giants derived in this study (cf. table 1) and those of 322 giants taken from Paper I, where the meanings of the symbols are the same as in figure 2. The theoretical solar-metallicity evolutionary tracks for $M = 1, 2, 3, 4, 5,$ and $6 M_{\odot}$ (PARSEC tracks; Bressan et al. 2012, 2013) are also depicted by solid lines (pre He-ignition) and dashed lines (post He-ignition) for comparison. See section 4 for estimations of probable $\log L$ ranges for 3 stars (HD 232862, KIC 9821622, and PDS 100).

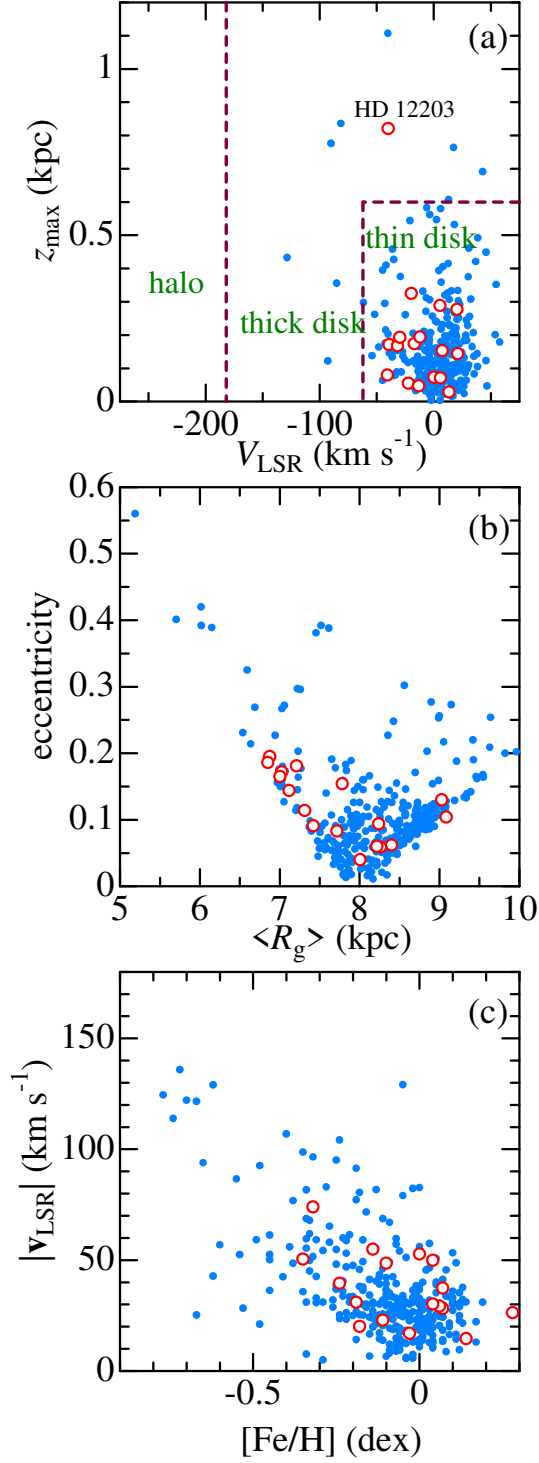


Fig. 5. Mutual correlations of kinematic parameters for 17 Li-rich giants (with available Hipparcos data) derived in this study and those of 322 giants taken from Paper I (where the meanings of the symbols are the same as in figure 2): (a) z_{\max} (maximum separation from the galactic plane) vs. V_{LSR} (rotation velocity component relative to LSR) diagram, which may be used for classifying the stellar population, (b) e (orbital eccentricity) vs. $\langle R_g \rangle$ (mean galactocentric radius) diagram, and (c) $[\text{Fe}/\text{H}]$ -dependence of the space velocity relative to LSR [$|v_{\text{LSR}}| \equiv (U_{\text{LSR}}^2 + V_{\text{LSR}}^2 + W_{\text{LSR}}^2)^{1/2}$].

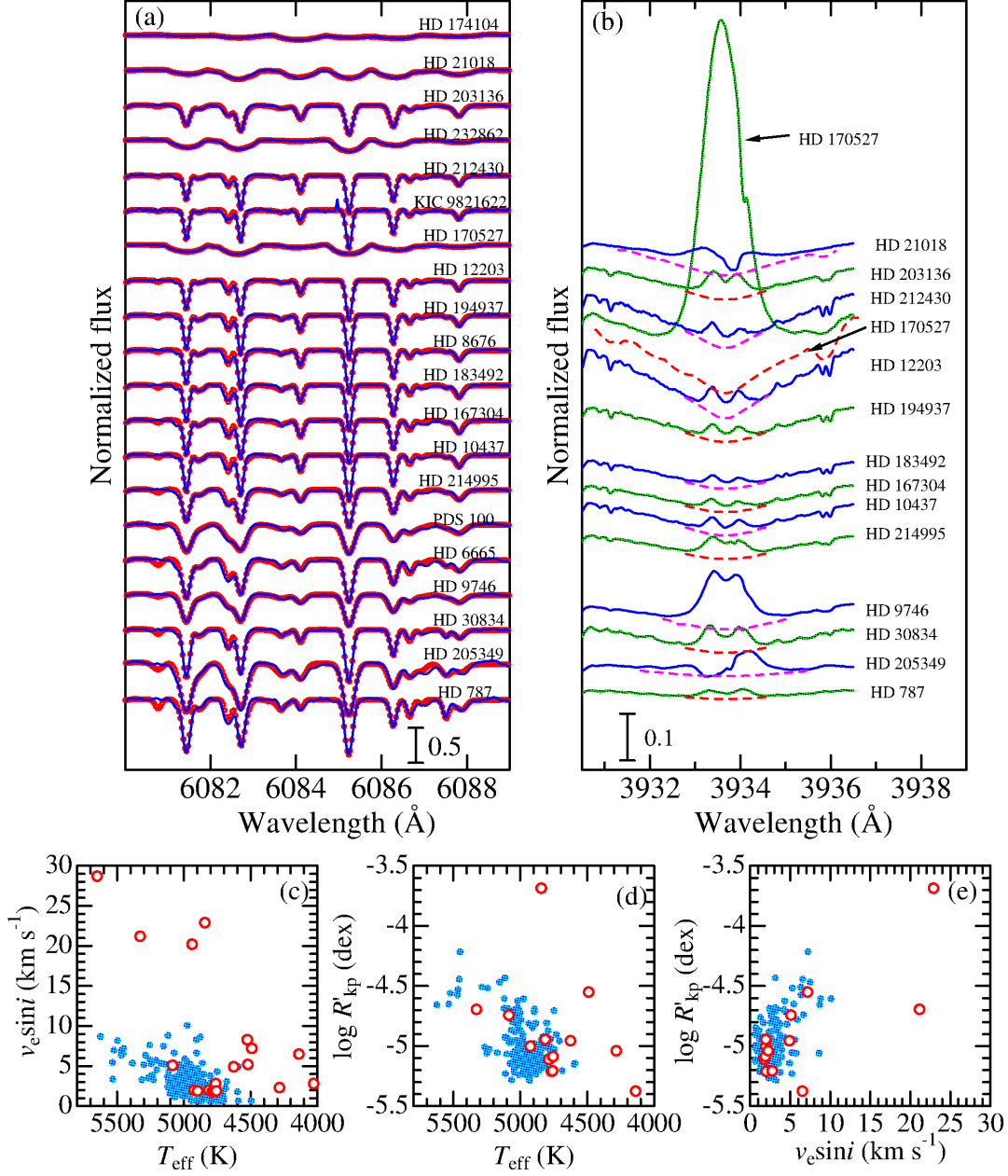


Fig. 6. (a) Synthetic spectrum fitting in the 6080–6089 Å region for evaluating $v_e \sin i$ for 20 program stars (see the caption of figure 7 for the meanings of the lines and symbols). (b) Display of the 3930–3937 Å region spectra (solid lines) including Ca II K line at 3933.663 Å for 17 Li-rich giants, for which UV spectra are available. The theoretical line profiles calculated from LTE photospheric model atmospheres are also overplotted by dashed lines in the core region $[w_{\min}, w_{\max}]$ where integration for evaluating the core-emission strength was performed. The wavelength scale is adjusted to the laboratory frame. Panels (c)–(e) show the mutual correlations between $\log R'_{\text{kp}}$ (activity indicator), $v_e \sin i$, and T_{eff} , where the meanings of the symbols are the same as in figure 2. Note that [number of Li-rich sample, number of normal sample] is [20, 322] in panel (c), while [14, 200] in panels (d) and (e) (because $\log R'_{\text{kp}}$ is involved).

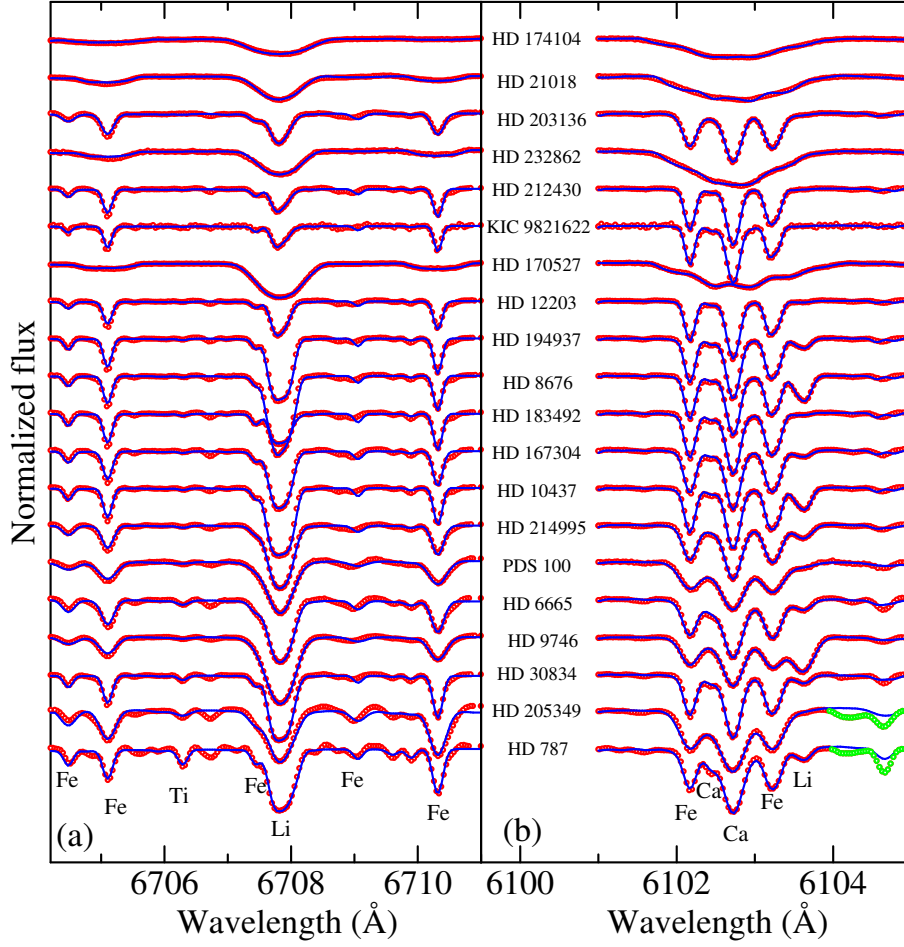


Fig. 7. Synthetic spectrum fitting in the 6704–6711 Å region comprising Li I 6708 line (left panel (a)) and 6101–6105 Å region comprising Li I 6104 line (right panel (b)) for determining the Li abundances of 20 program stars (arranged in the descending order of T_{eff} as in table 1). The observed spectra are plotted in red symbols (where the masked regions discarded in judging the goodness of fit are colored in light-green) while the best-fit theoretical spectra are shown in blue solid lines. The wavelength scale is adjusted to the laboratory system.

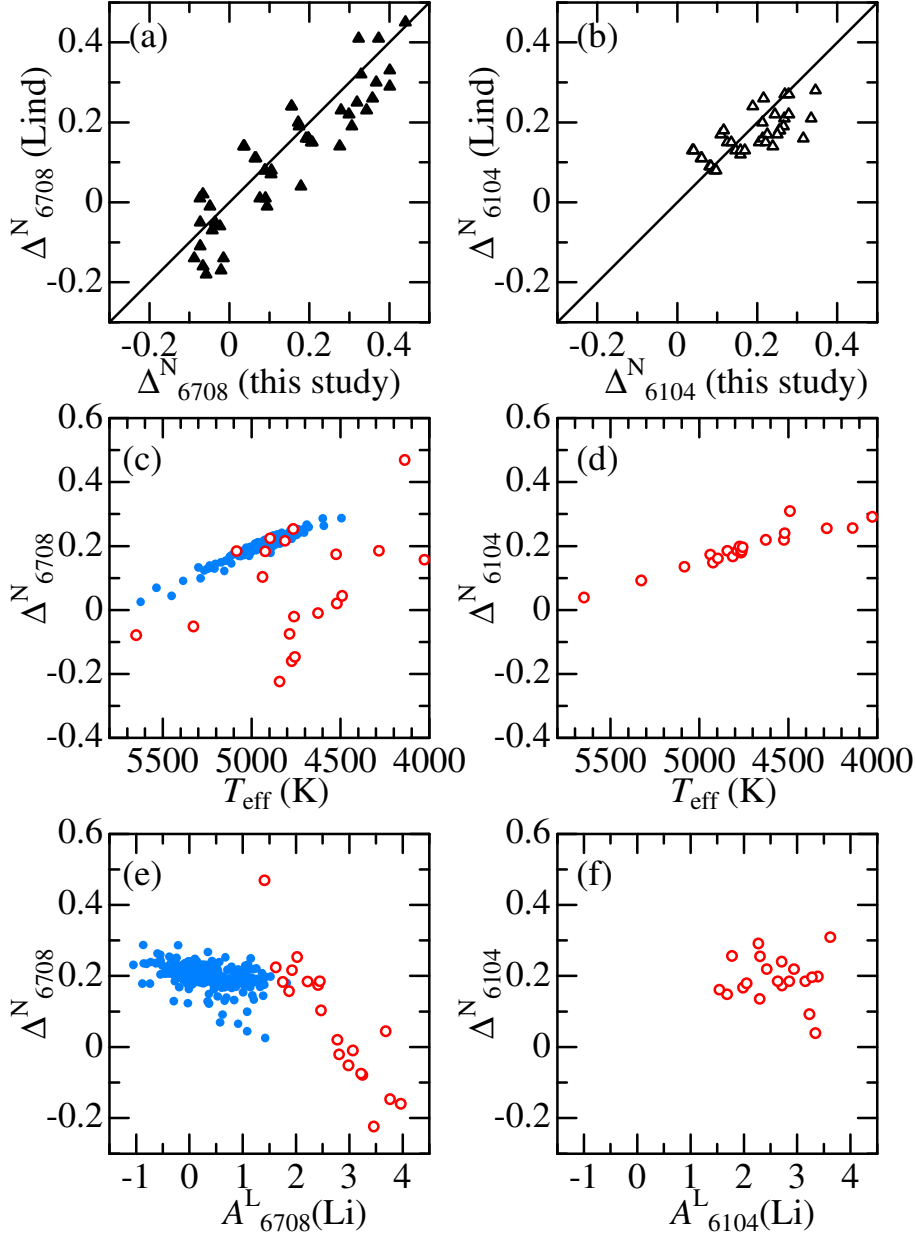


Fig. 8. The top panels (a, b) compare our non-LTE corrections of Li lines (Δ^N) computed for 48 models ($v_t = 2 \text{ km s}^{-1}$ case with combinations of $T_{\text{eff}} = 4000, 4500, 5000 \text{ K}$; $\log g = 1, 2, 3, 4$; and $A^L(\text{Li}) = 1.5, 3.0$) with those published by Lind et al. (2009). In the middle (c, d) and bottom (e, f) panels are plotted our Δ^N results derived for actual stars against T_{eff} and $A^L(\text{Li})$ (LTE abundance), respectively. The left-hand and right-hand panels correspond to the results for Li I 6708 line and Li I 6104 line, respectively. Regarding the four panels (c)–(f), the same meanings of the symbols as in figure 2.

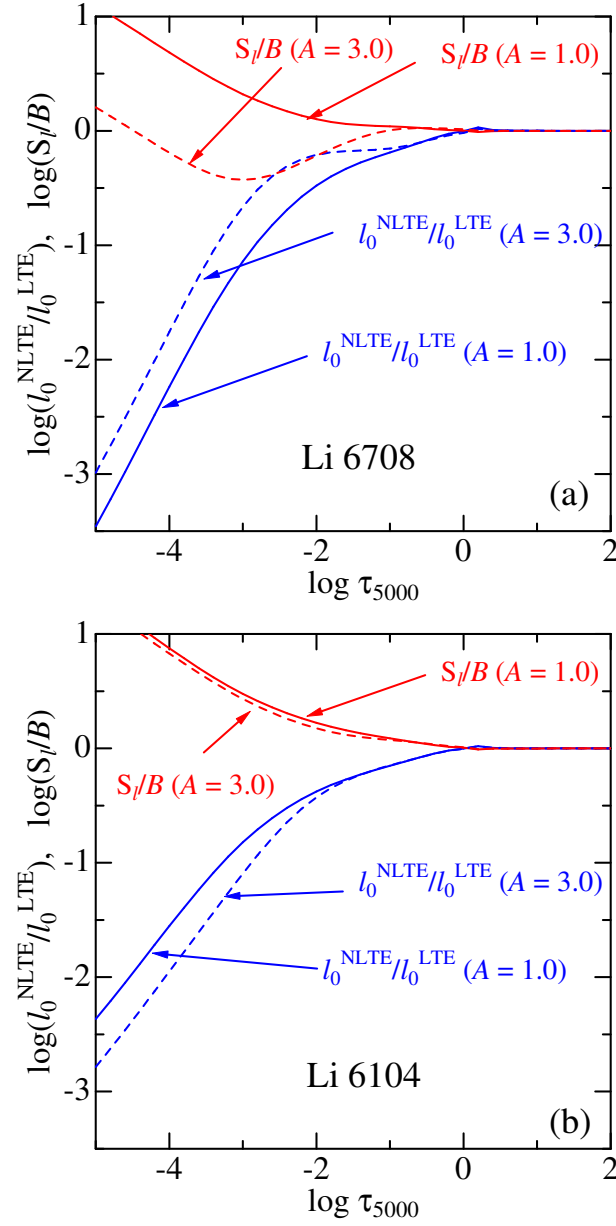


Fig. 9. Ratio of the Li I line source function (S_L) to the local Planck function (B) and the NLTE-to-LTE line-center opacity ratio as functions of the standard continuum optical depth at 5000 Å, which were computed for the solar-metallicity model of $T_{\text{eff}} = 4500$ K and $\log g = 2.0$ with two different Li abundances of $A(\text{Li}) = 1$ (dashed line) and 3 (solid line). The red and blue lines correspond to S_L/B and $l_0^{\text{NLTE}}/l_0^{\text{LTE}}$, respectively. Upper panel (a): $2s \ ^2S - 2p \ ^2P^\circ$ transition of multiplet 1 (corresponding to Li I 6708). Lower panel (b): $2p \ ^2P^\circ - 3d \ ^2D$ transition of multiplet 4 (corresponding to Li I 6104).

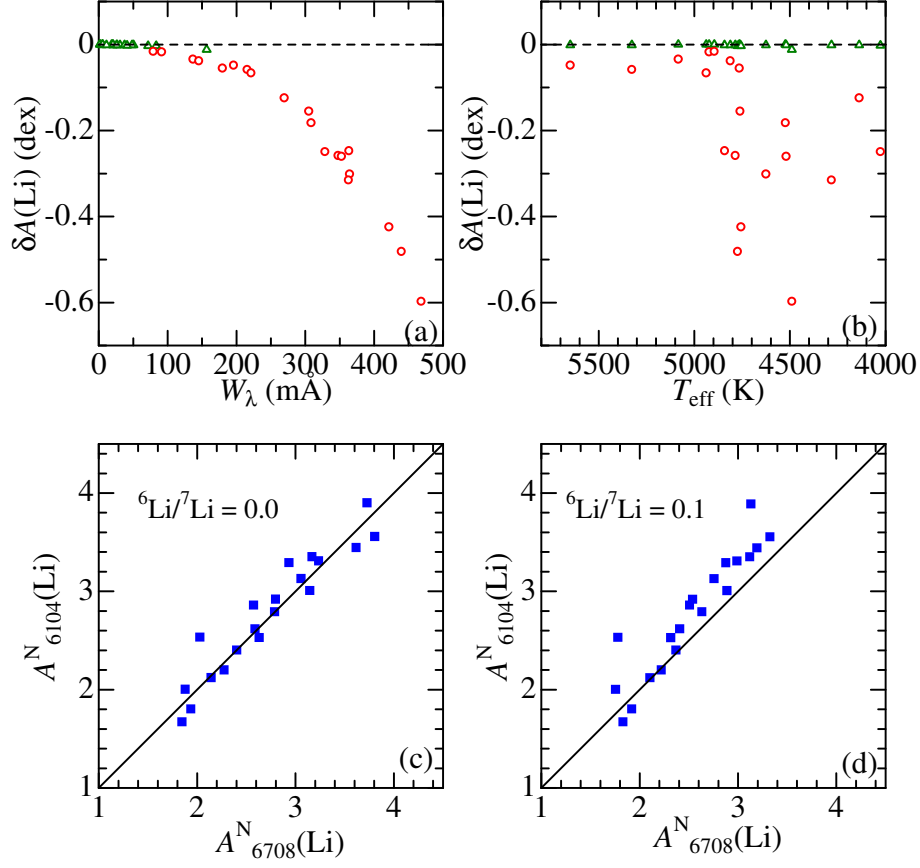


Fig. 10. In the upper panels (a) and (b) are plotted $\delta A(\text{Li})$ against W_λ and T_{eff} , respectively, where $\delta A(\text{Li})$ is the (non-LTE) Li abundance variation caused by including ${}^6\text{Li}$ with the isotope ratio of ${}^6\text{Li}/{}^7\text{Li} = 0.1$ in comparison to the standard case of neglecting ${}^6\text{Li}$. The open circles and open triangles correspond to Li I 6708 and Li I 6104, respectively. The lower two panels show how $A_{6104}^N(\text{Li})$ vs. $A_{6708}^N(\text{Li})$ correlation is affected by inclusion of ${}^6\text{Li}$. (c) — ${}^6\text{Li}/{}^7\text{Li} = 0.0$ (no ${}^6\text{Li}$), (d) — ${}^6\text{Li}/{}^7\text{Li} = 0.1$.

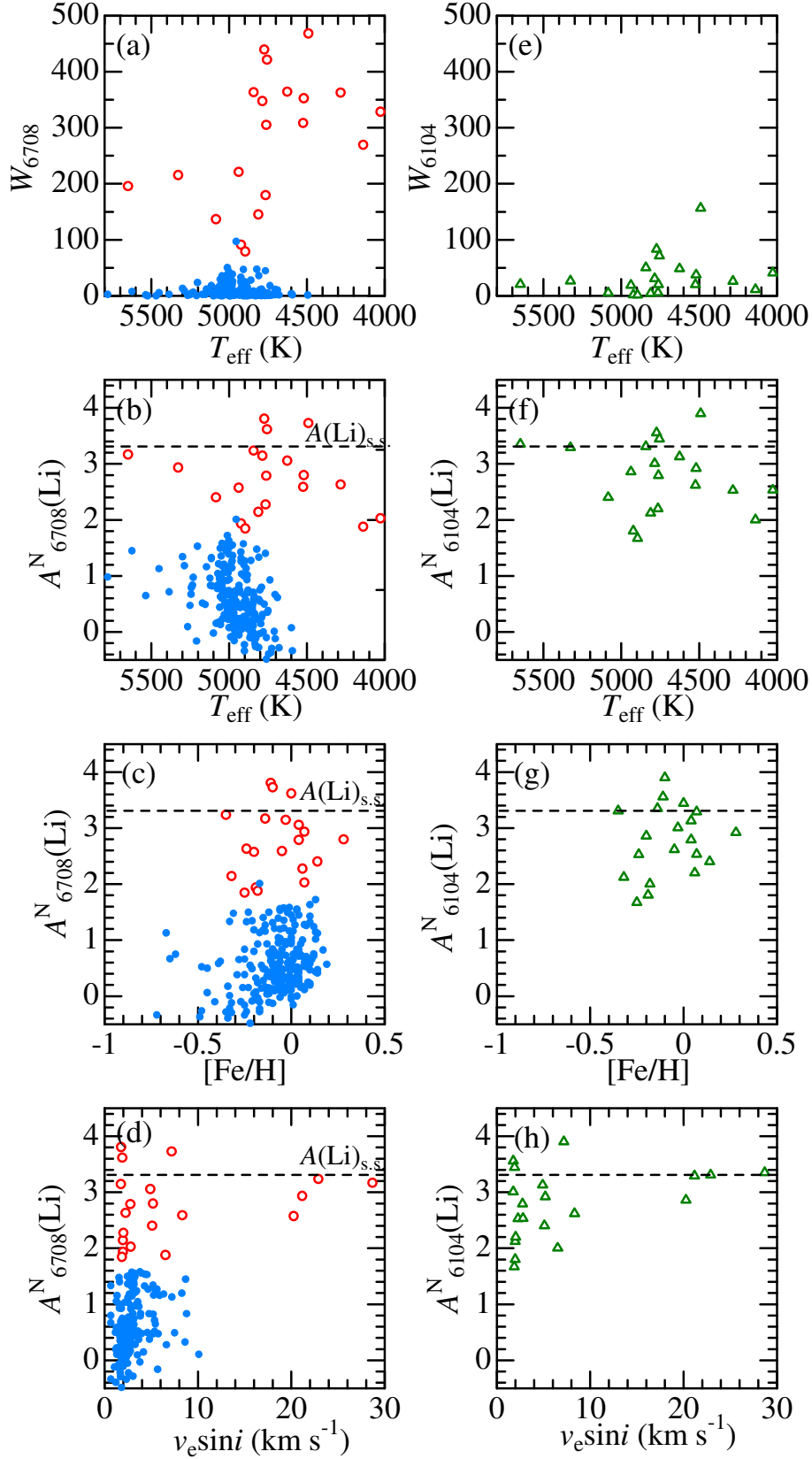


Fig. 11. Behaviors of W (equivalent width of Li line feature) and $A^N(\text{Li})$ (non-LTE Li abundance) in terms of the stellar parameters. The left-hand panels show the results for the Li i 6708 line: (a) W_{6708} vs. T_{eff} , (b) $A^N_{6708}(\text{Li})$ vs. T_{eff} , (c) $A^N_{6708}(\text{Li})$ vs. $[\text{Fe}/\text{H}]$, and (d) $A^N_{6708}(\text{Li})$ vs. $v_e \sin i$. The right hand panels (e)–(h) (each corresponding to panels (a)–(d), respectively) are for the cases of the Li i 6104 line. The horizontally drawn dashed line indicates the solar-system Li abundance (3.31). The results for 20 Li-rich giants and those for 239 normal giants (cf. appendix 2) are shown by open and filled symbols, respectively.

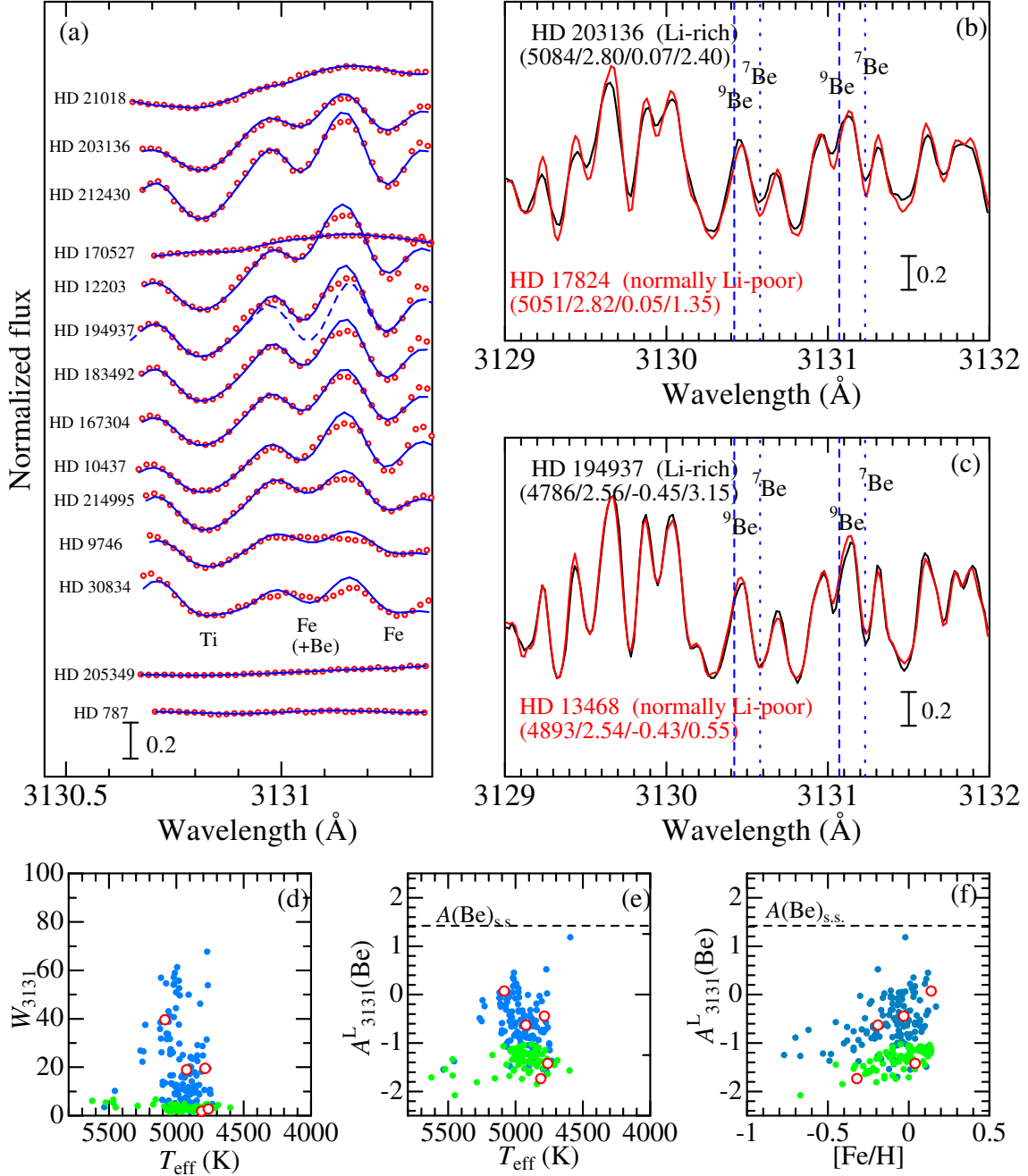


Fig. 12. (a) Synthetic spectrum fitting in the 3130.65–3131.35 Å region for Be abundance determination. Note that although the $A(\text{Be})$ solution was converged only for 5 stars (HD 203136, HD 212430, HD 12203, HD 194937, and HD 167304), the fitting was anyway accomplished also for unsuccessful cases by fixing $A(\text{Be})$ at a negligible level. For HD 194937, an additional theoretical spectrum simulated for $A(\text{Be}) = 1.42$ (solar-system Be abundance) is also depicted in dashed line, in order to show the difference compared with the best-fit spectrum of $A(\text{Be}) = -0.44$ (solid line). Otherwise, the same as in figure 7. In panels (b) and (c) are compared the 3129–3132 Å region spectra of two Li-rich giants (HD 203136 and HD 194937; black lines) with those of normal giants of similar parameters (HD 17824 and HD 13468; red lines), respectively. [$T_{\text{eff}}/\log g/A^L(\text{Be})/A^N(\text{Li})$ are indicated for each star in the figure, and the positions of stable ^9Be as well as unstable ^7Be doublet lines are indicated by vertical dashed and dotted lines, respectively.] Panels (d), (e), and (f) show the W_{3131} vs. T_{eff} , $A^L(\text{Be})$ vs. T_{eff} , and $A^L(\text{Be})$ vs. $[\text{Fe}/\text{H}]$ relations, respectively, where the meanings of the symbols are almost the same as in figure 2 (but the filled circles for normal giants colored in light-green indicate the upper limits) and the horizontal dashed line indicates the solar-system Be abundance of 1.42.

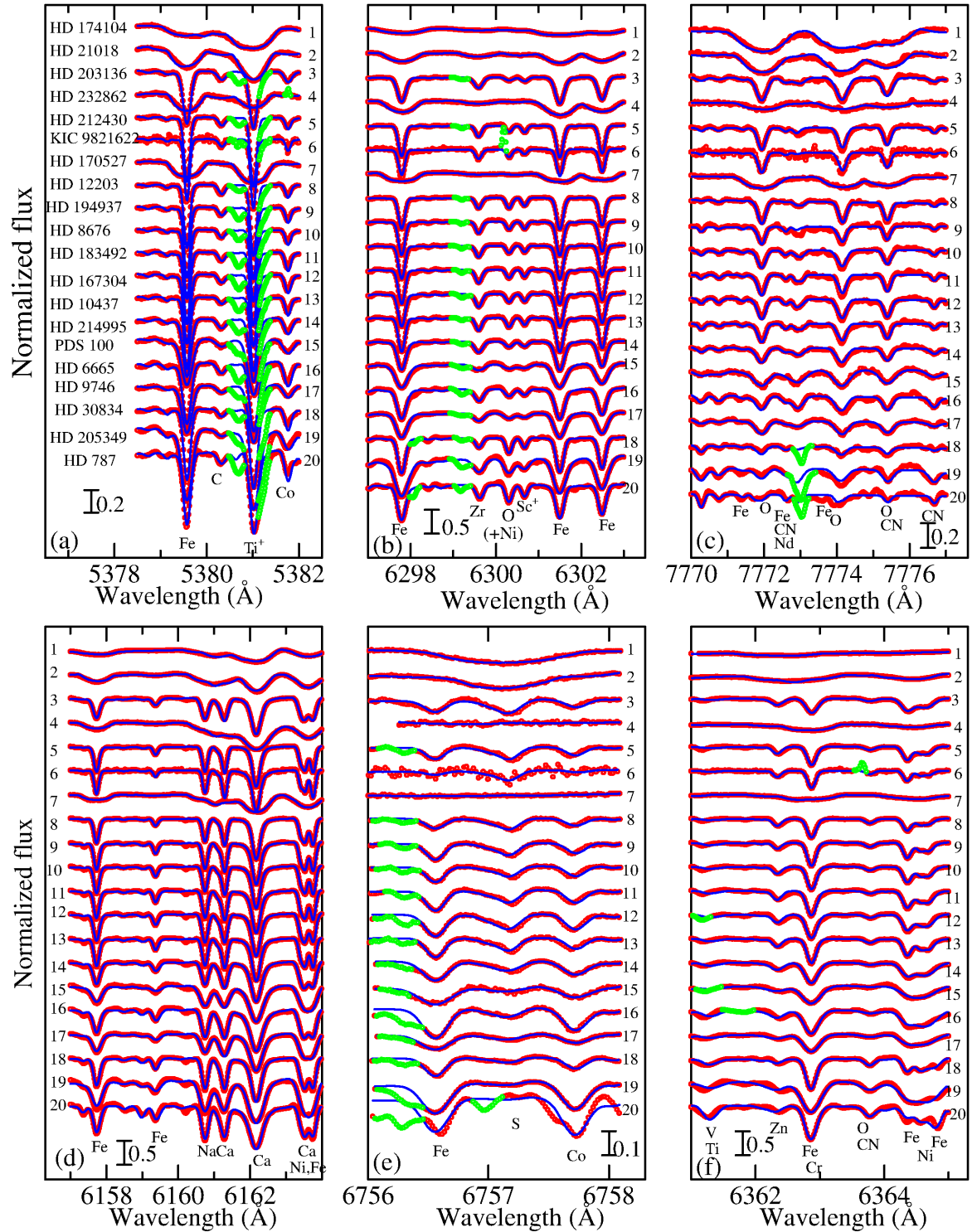


Fig. 13. Synthetic spectrum fitting carried out for determining the abundances of C, O, Na, S, and Zn. (cf. table 2). (a) 5378.5–5382 Å region comprising C I 5380, (b) 6297–6303 Å region comprising [O I] 6300, (c) 7770–7777 Å region comprising O I 7771–5, (d) 6157–6164 Å region comprising Na I 6161, (e) 6756.0–6758.1 Å region comprising S I 6757, and (f) 6361–6365 Å region comprising Zn I 6362. Otherwise, the same as in figure 7. Note that the telluric lines in the 6297–6303 Å region and the broad Ca I autoionization feature in the 6361–6365 Å region were removed by dividing the spectra by appropriate references.

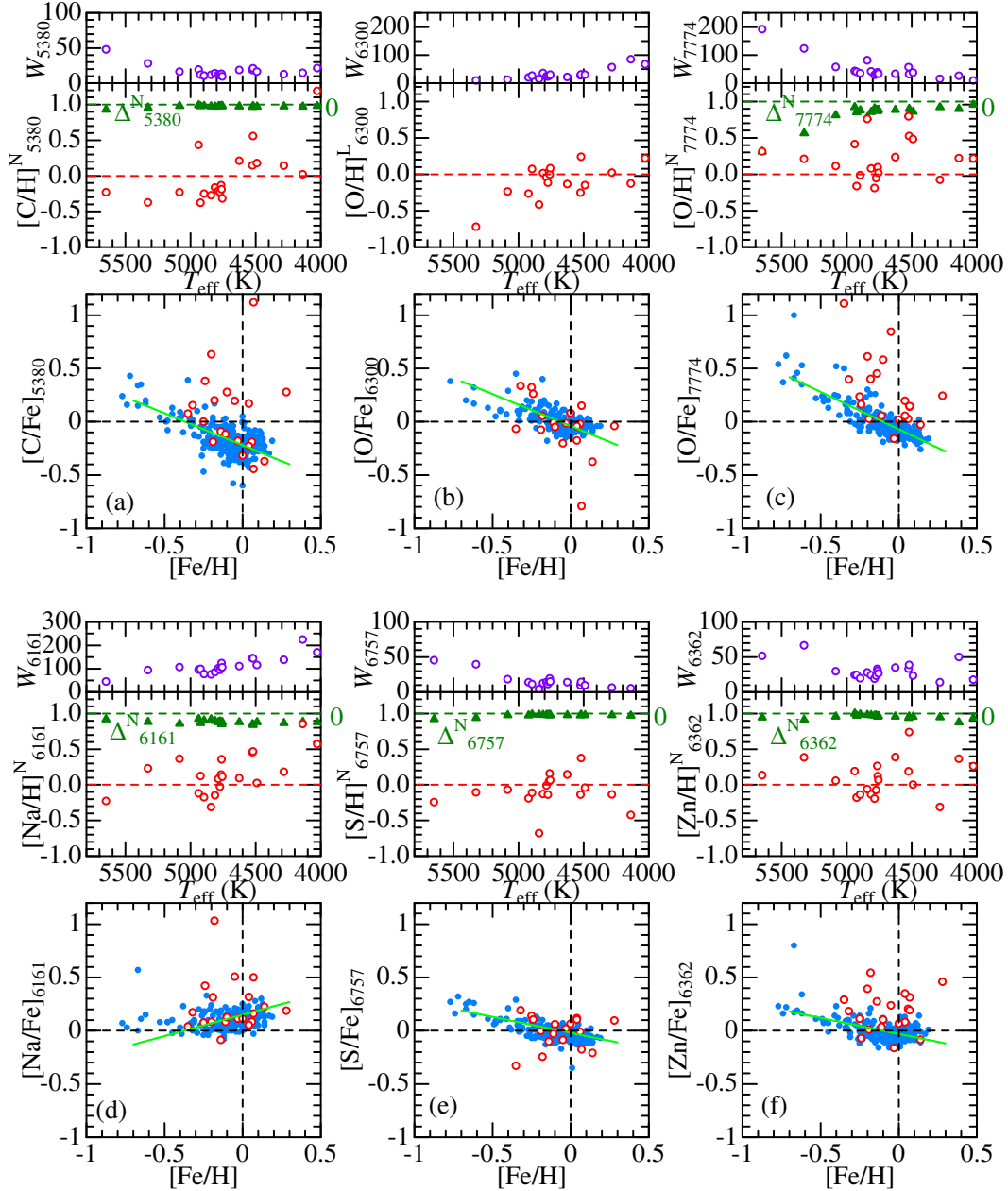


Fig. 14. Each of the 6 figure sets (a–f) consist of 3 panels (tentatively named t, m, b as abbreviations of “top”, “middle”, and “bottom”), where the results of C, O, Na, S, and Zn abundances ($[X/H]$... panel-m, $[X/Fe]$... panel-b), equivalent widths (W ... panel-t), and non-LTE corrections (Δ^N ... panel-m) plotted against T_{eff} (panel-t and panel-m) or $[Fe/H]$ (panel-b). Here, as in figure 2, the open and filled circles correspond to Li-rich giants and normal giants, respectively. (a) C I 5380, (b) O I 7774, (d) Na I 6161, (e) S I 6757, and Zn I 6362. Note that the origin of Δ^N (shown by filled triangles) is marked in the right ordinate of panel-m. The (light-green) straight line drawn in panel-b is the approximate mean relation for the normal giants (filled circles).

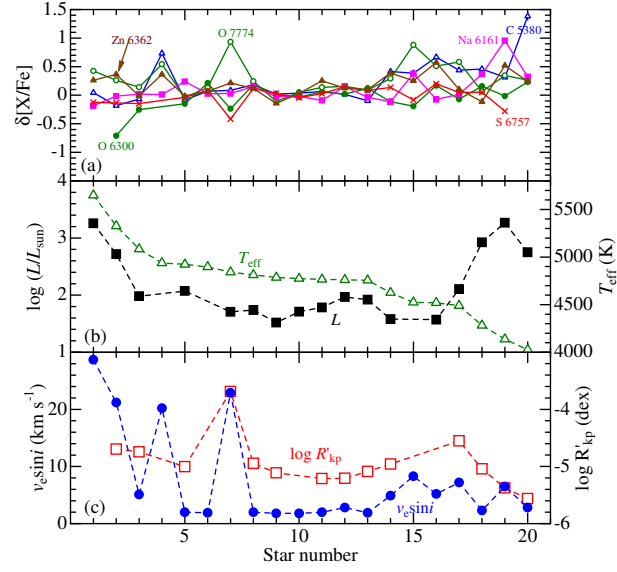


Fig. 15. (a) Deviations of $\delta[X/Fe]$ ($\equiv [X/Fe] - [X/Fe]_{\text{mean}}$) are plotted against the star number (in the order of decreasing T_{eff}). Open triangles (blue) — C I 5380, filled circles (green) — [O I] 6300, open circles (green) — O I 7774, filled squares (pink) — Na I 6161, crosses (red) — S I 6757, and filled triangles (brown) — Zn I 6362. (b) $\log(L/L_{\odot})$ (filled squares) and T_{eff} (open triangles) plotted against the star number. (c) $v_e \sin i$ (filled circles) and $\log R'_{\text{kp}}$ (open squares) plotted against the star number.

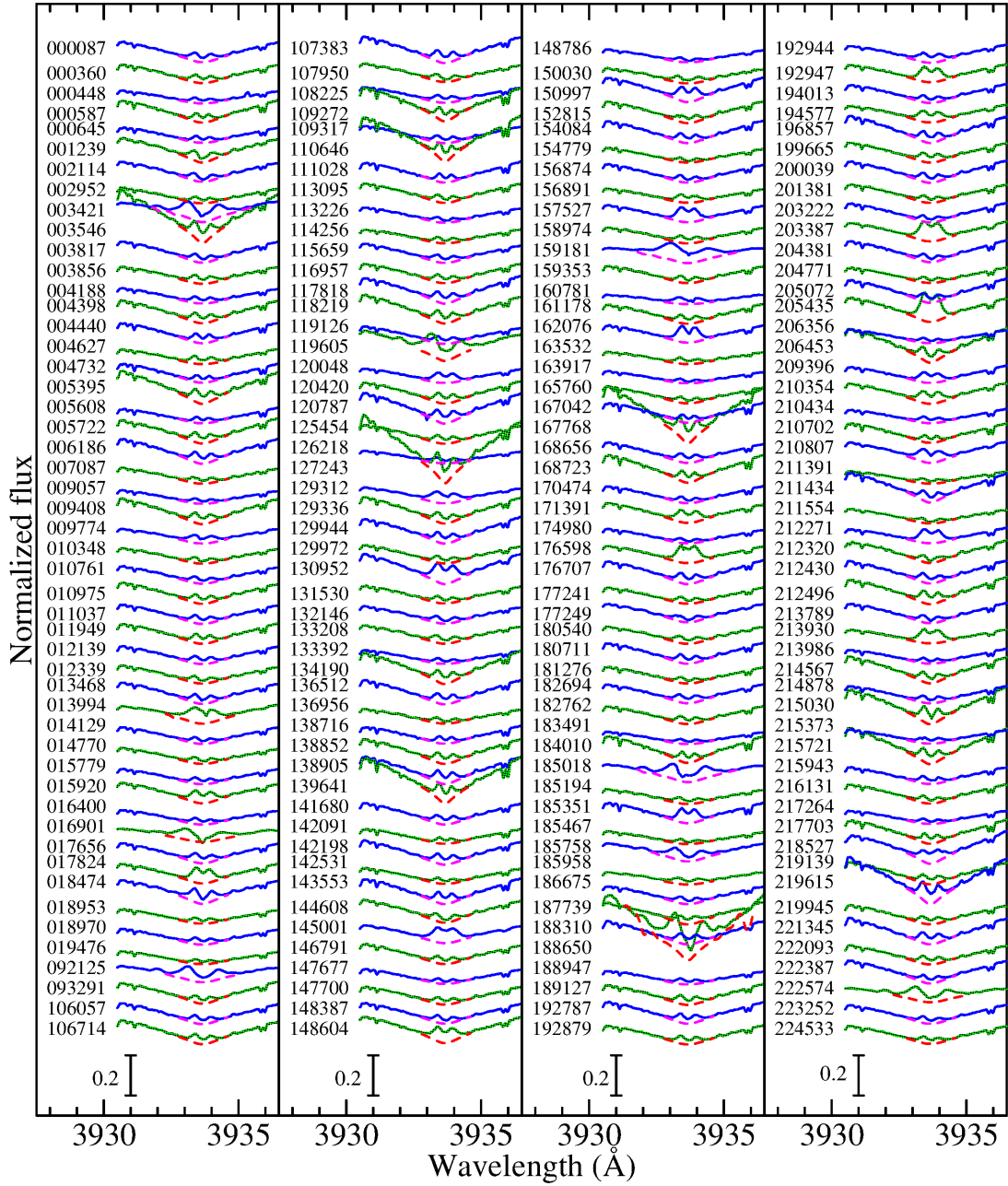


Fig. 16. Display of the 3930.5–3936.5 Å region spectra (solid lines) of Ca II K line at 3933.663 Å for all the 200 giants studied in Paper II. In addition, theoretical LTE line profiles (r_{λ}^{th}) calculated from the model atmospheres are also overplotted by dashed lines in the core region [w_{\min} , w_{\max}], where integration was done for evaluating the emission strength. Each spectrum is vertically shifted by 0.1 (in continuum unit) relative to the adjacent one. The wavelength scale of all stellar spectra is adjusted to the laboratory frame by correcting the radial velocity shifts. The HD numbers are indicated in the figure. Regarding several lower-metallicity stars, more sharply V-shaped wings tend to cross the spectra of other stars, which makes their identification confusing. In such cases, it is recommended to pay attention (not to the line wing but) to the line center of the theoretical profile (dashed line).

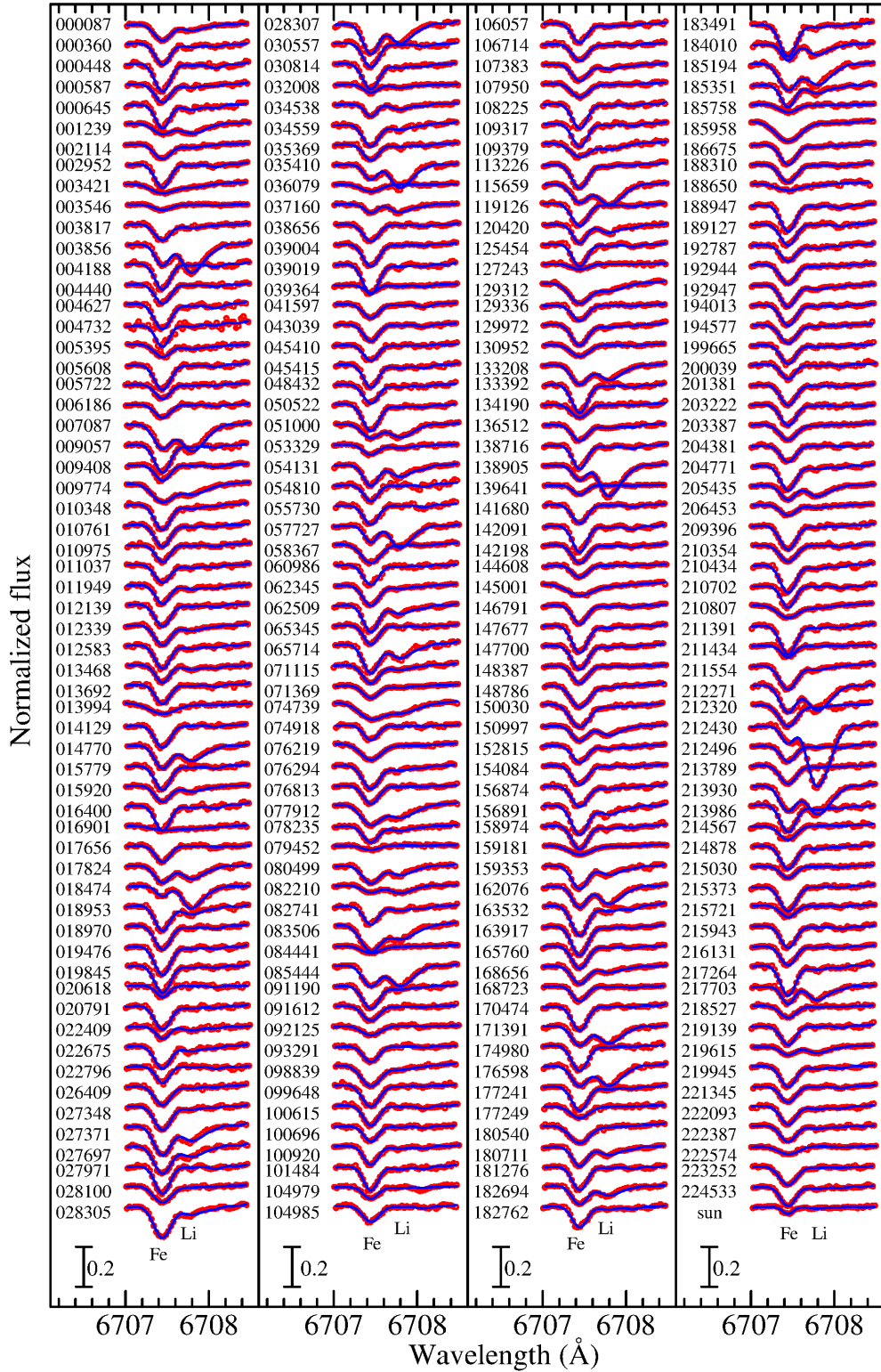


Fig. 17. Synthetic spectrum analysis of the 6707.0–6708.5 Å region including lines of Li I and Fe I for 239 giants studied in Paper III (note that only HD 212430 is in common with our sample of 20 Li-rich giants). The best-fit theoretical spectra are shown by solid lines, while the observed data are plotted by symbols. A vertical offset of 0.1 is applied to each spectra relative to the adjacent ones. The HD numbers are indicated in the figure. Note that fitting was somehow accomplished even for unsuccessful cases (i.e., Li abundance solution could not be established because the line is too weak) by fixing the contribution of Li I 6708 line at a negligible level.

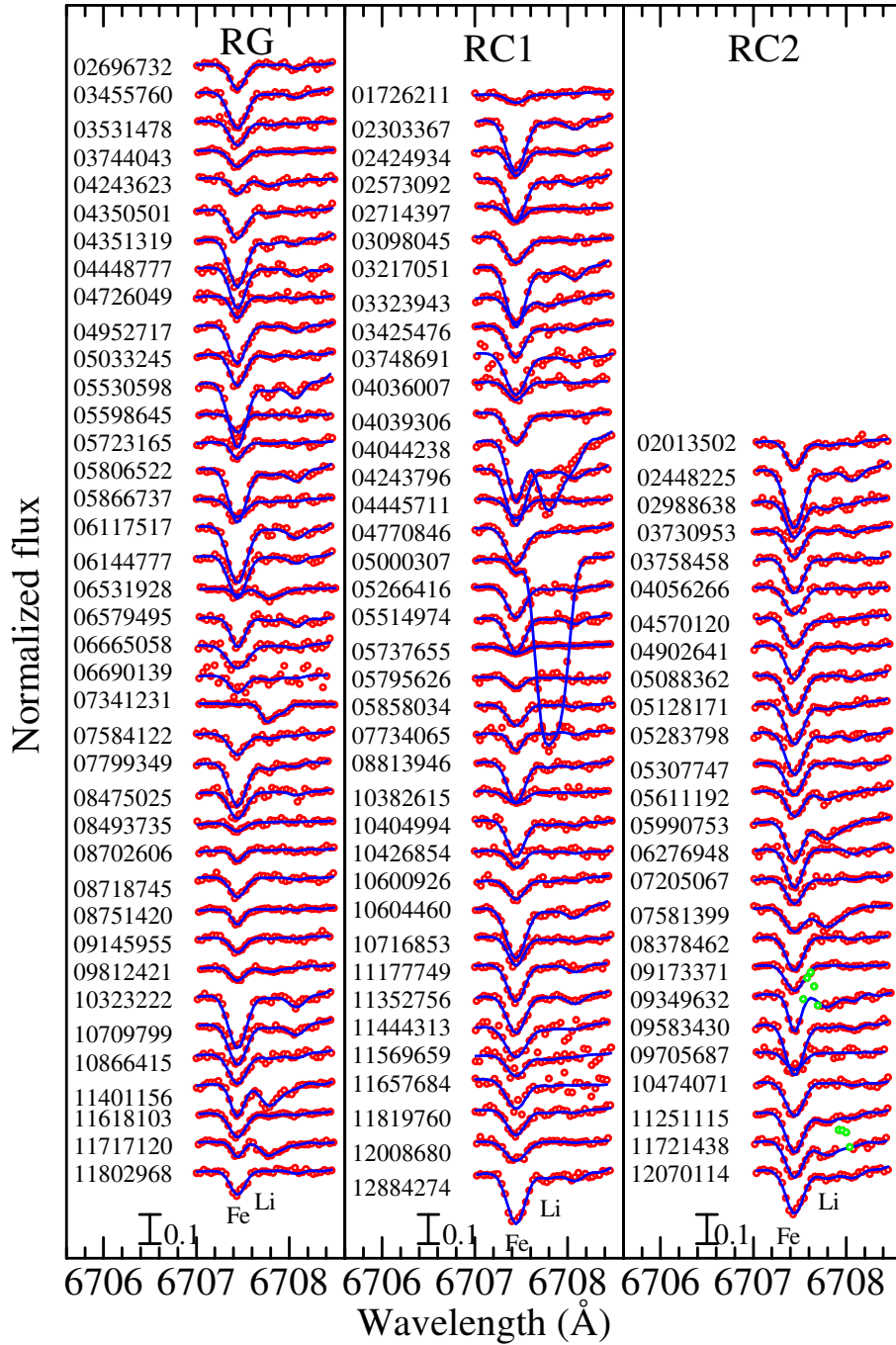


Fig. 18. Synthetic spectrum analysis of the 6707.0–6708.5 Å region for 103 giants in the *Kepler* field studied by Takeda and Tajitsu (2015) and Takeda et al. (2016a), for which the evolutionary status is asteroseismologically established. The left, center, and right panel corresponds to RG (red giants ascending the RGB), RC1 (1st clump giants), RC2 (2nd clump giants), respectively. The KIC numbers are indicated in the figure. Otherwise, the same as in figure 17.

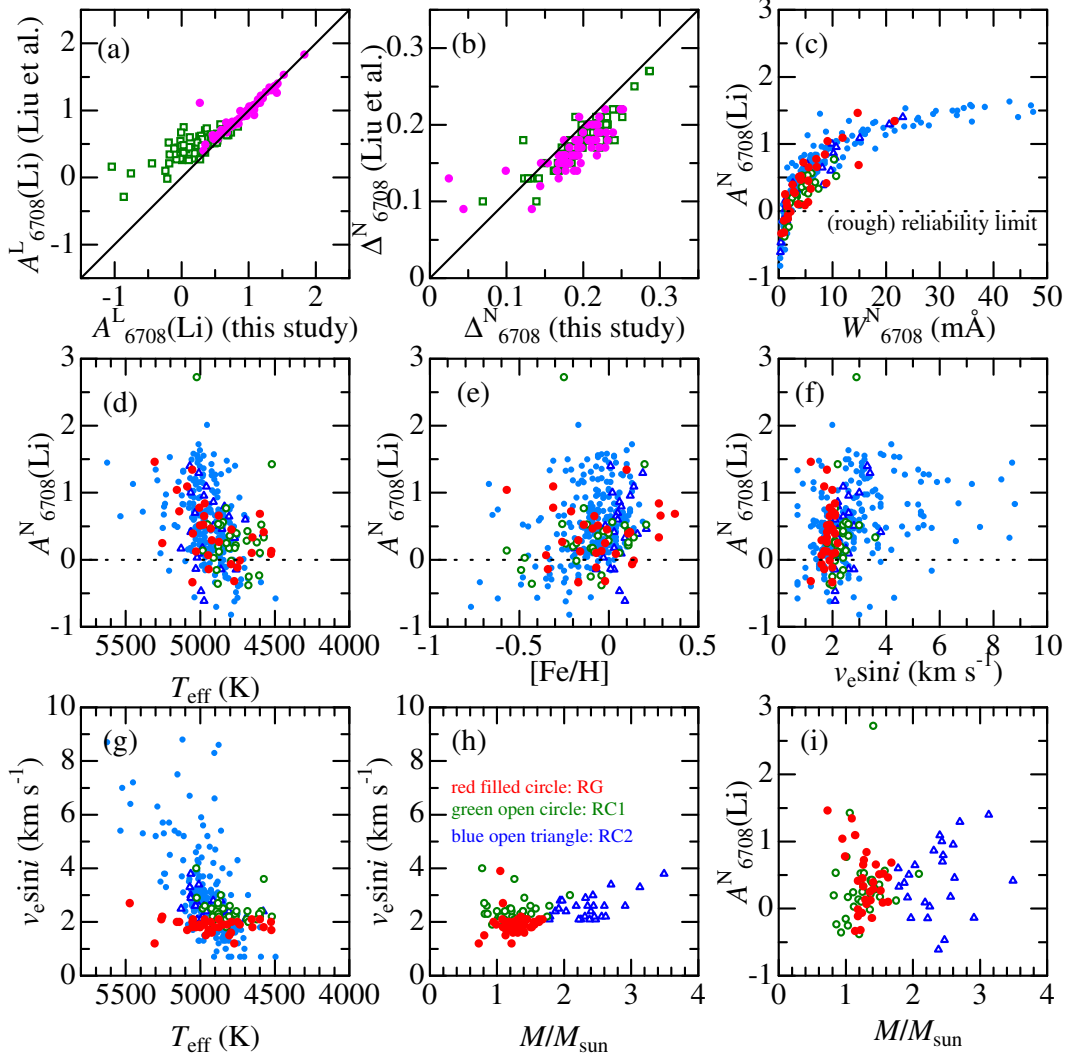


Fig. 19. Panels (a) and (b) compare our lithium abundances and the corresponding non-LTE corrections determined for 239 giants with those derived by Liu et al. (2014), where filled and open symbols correspond to the subsample group A1 (clear Li detection) and A2 (undistinguished Li detection) defined by them, respectively. Panels (c)–(i) illustrate the trend of Li abundances (along with the equivalent widths and stellar parameters) of 239 giants (blue smaller filled circles) and 103 *Kepler* field giants (red larger filled circles — RG, green open circles — RC1, and blue open triangles — RC2): (c) A_{6708}^N vs. W_{6708}^N , (d) A_{6708}^N vs. T_{eff} , (e) A_{6708}^N vs. $[\text{Fe}/\text{H}]$, (f) A_{6708}^N vs. $v_e \sin i$, (g) $v_e \sin i$ vs. T_{eff} , (h) $v_e \sin i$ vs. M , and (i) A_{6708}^N vs. M . Note that the lithium abundances are reliable only above the critical limit of $A(\text{Li}) \sim 0$ (shown by the dotted line, corresponding to W_{6708} of a few mÅ), below which the apparent $A(\text{Li})$ values should not be seriously taken.